Thermochemical Analysis of Gas-Cooled Reactor Fuels Containing Am and Pu Oxides

September 2002

Prepared by
T. B. Lindemer

THERMOCHEMICAL ANALYSIS OF GAS-COOLED REACTOR
FUELS CONTAINING Am AND Pu OXIDES

T. B. Lindemer*

* Consultant: Harbach Engineering and Solutions, Inc., 8807 Fox Hollow Court, Dayton OH 45458

Date Published: September 2002

CONTENTS

LIST OF FIGURES

LIST OF TABLES

EXECUTIVE SUMMARY

The primary purpose of this review is to guide the Advanced Fuel Cycle Initiative (AFCI) activities of the U.S. Department of Energy (DOE) in the planning and development of coated particle fuels for transmutation applications. The present focus is on fuels to support the Deep-Burn Modular Helium Reactor (MHR) concept. Other AFCI fuels applications, and other DOE programs may find this review useful. Primary thermochemical questions related to the viability of coated particle fuels containing Pu and Am are addressed in this report. The primary findings of this report are as follows:

- Volatility losses of Pu can be kept acceptably low for fuel manufacture in both oxide and oxycarbide fuel kernels.

- Volatility losses of Am can be kept acceptably low in oxide systems, but will likely be unacceptably high in an oxycarbide fuel kernel.

- Large CO pressures are likely to develop in substoichiometric oxide kernels at the highest burnups (75% FIMA) anticipated for the Deep Burn MHR.

- Oxycarbide kernels can totally suppress CO formation at even the highest burnups of the Deep Burn MHR.

Other findings relate to the need for additional work on the interaction of fission metals (Ag, Pd, Ru) with SiC and ZrC coatings, and the potential for ZrC to be used as an oxygen getter in TRISO fuel designs.

ACKNOWLEDGEMENT

THERMOCHEMICAL ANALYSIS OF GAS-COOLED REACTOR
FUELS CONTAINING Am AND Pu OXIDES

T. B. Lindemer

ABSTRACT

Literature values and estimated data for the thermodynamics of the actinide oxides and fission products are applied to explain the chemical behavior in gas-cooled-reactor fuels. Emphasis is placed on the Am-O-C and Pu-O-C systems and the data are used to plot the oxygen chemical potential versus temperature of solid-solid and solid-gas equilibria. These results help explain observations of vaporization in Am oxides, nitrides, and carbides and provide guidance for the ceramic processing of the fuels. The thermodynamic analysis is then extended to the fission product systems and the Si-C-O system. Existing data on oxygen release (primarily as CO) as a function of burnup in the thoria-urania fuel system is reviewed and compared to values calculated from thermodynamic data. The calculations of oxygen release are then extended to the plutonia and americia fuels. Use of ZrC not only as a particle coating that may be more resistant to corrosion by Pd and other noble-metal fission products, but also as a means to getter oxygen released by fission is discussed.

---

1. INTRODUCTION

The present Oak Ridge National Laboratory and General Atomics cooperative effort (ref. ro02) to develop a new gas-cooled reactor type requires a 95%Pu-5%Np driver fuel (DF) and a 60%Pu-5%Np-30%Am-5%Cm transmutation fuel (TF). Experience shows that Am-containing systems often exhibit Am loss at usual ceramic processing temperatures; to a lesser extent, the Pu-O system can exhibit similar behavior. These losses must be understood and controlled to permit fuel kernel synthesis and manufacture of a TRISO-coated[1] fuel, and the in-particle Am-containing vapor species present during reactor operation need to be defined. The thermodynamic data in the literature and estimated data are used to rationalize the observed Am losses, to give processing guidance for kernel fabrication, and to predict changes in the chemical potential of oxygen, (primarily as increases in CO pressure) during fuel burnup in-reactor. The thermodynamic behavior of these systems is represented mathematically and graphically.

2. THE ELLINGHAM DIAGRAM

The Ellingham diagram of Fig. 1 is for the Am-O system as developed below and it is similar to those of many metal oxide systems (ref. da53). The diagram illustrates several thermodynamic quantities relevant to metal oxide systems. The vertical axis is the chemical potential of oxygen and is fundamental to the present analysis. It is $RTln(p*[O_2])$, in which R is the gas constant, 1.987 cal mol^{-1} K^{-1}, T is temperature (K), and $p*[O_2]$ is the equilibrium partial pressure of oxygen divided by the partial pressure of oxygen in the standard state of one atmosphere or 0.101 Mpa. By this convention, $p*[O_2]$ (as well as all other gaseous partial pressures) is a dimensionless number that has the numerical value of the pressure in atmospheres.

---

[1] TRISO coatings consist of inner pryocarbon layers over a spherical fuel kernel, a SiC layer, and an outer pyrocarbon layer.
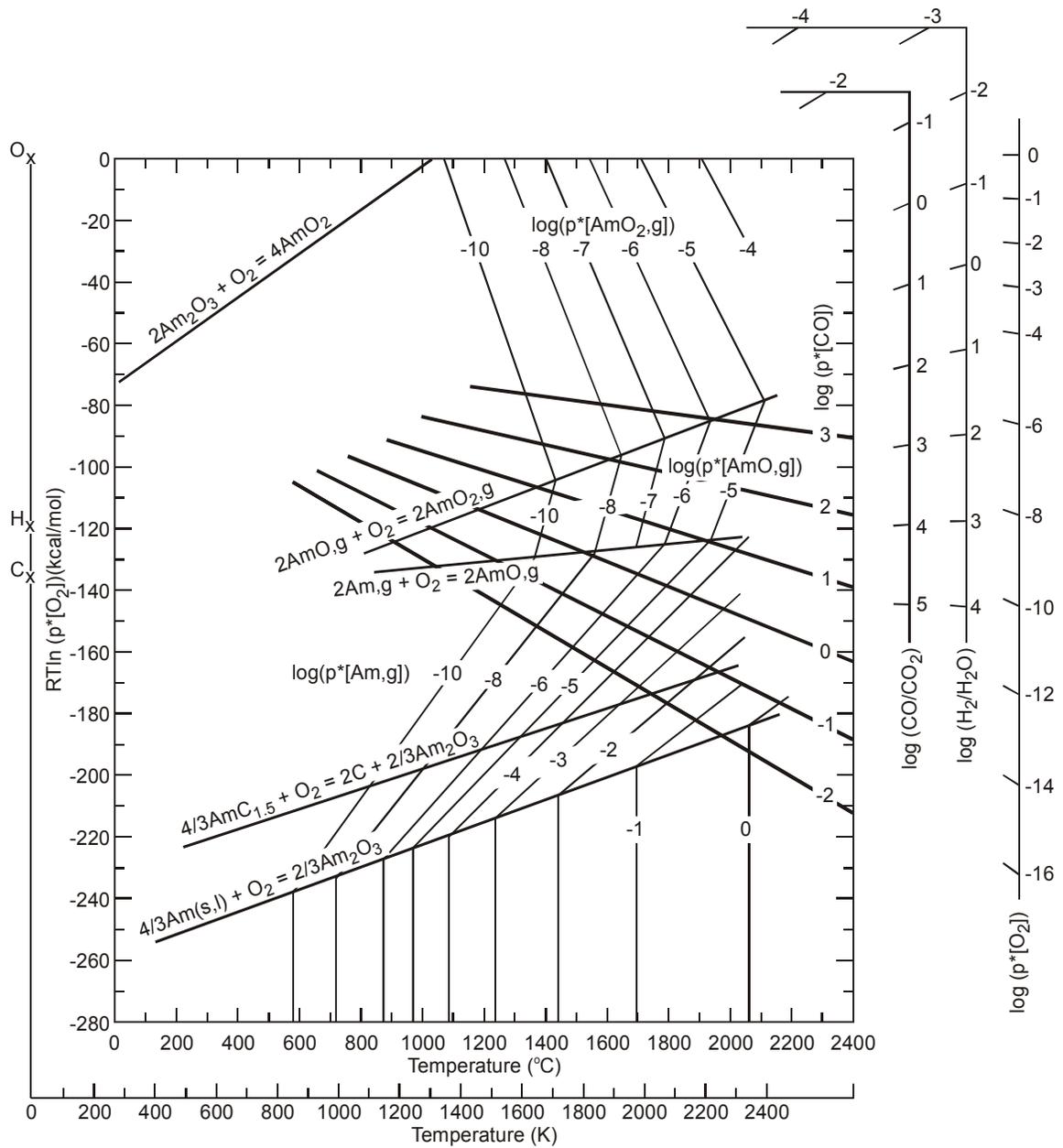
Fig. 1. The Ellingham diagram for the Am-O-C system. (The oxygen potentials for the Am,g-AmO,g and AmO,g-AmO$_2$,g equilibria are plotted where the two pressures in each equilibrium are equal.)

The Ellingham diagram is also a nomograph. The vertical line to the left is at absolute zero and is marked with "O", "H" and "C". A straightedge, when placed on "O" and any illustrated equilibrium at a given temperature, extends to the right-hand side of the figure and permits an approximate reading of $p*[O_2]$ for that equilibrium at that temperature. Similarly, "H" and "C" are used to find the H_2/H_2O and CO/CO_2 values, respectively, and are related to $p*[O_2]$ and oxygen potential by the equilibria $2 H_2 + O_2 = 2 H_2O$ and $2 CO + O_2 = 2 CO_2$, respectively. Additional Ellingham diagrams will be developed here to illustrate thermodynamic characteristics relevant to the processing and in-reactor behavior of the DF and TF fuels.

Several primary sources of thermodynamic data were used during construction of the Ellingham diagrams. Probably the best comprehensive single source of thermodynamic data for metals and their oxides is the publication by Pankratz (ref. pa82). Hultgren et. al. (ref. hu73) is a similar comprehensive source for the metals and provides an analysis of the original data. Cordfunke et. al. (ref. co90) provide analysis and data for the americium oxides and Cs-Mo-O compounds; their data are used here for Am gas because their analysis supercedes that in ref. hu73. The JANAF (ref. st71) tables were used for data for the C-O, H-O, Si-O and Si-C systems. In the case of the data for actinide systems, the most recent reference was used if it was based on newer analyses. Brewer and Rosenblatt (ref. br61) provide a comprehensive review for metal dioxide gases, Pedley and Marshall (ref. pe83) treat the metal monoxide gases, and Lamoreaux et. al. (ref. la87) analyze the vaporization of metal oxides and illustrate the method for calculating the conditions for congruent evaporation.

3. THE C-CO SYSTEM

The C-CO system is basic to gas-cooled reactor fuels systems because it is fundamental to both carbothermic conversion of oxides to carbides for the fuel kernels and to generation of in-particle CO pressure during fission of an actinide oxide fuel kernel. The thermodynamic calculations for the system are also used here to illustrate the general approach to all the calculations to be used in this text. The oxygen potential is obtained for any equilibrium by writing the latter in terms of one mole of oxygen, e.g.,

$$2 C + O_2 = 2 CO \tag{3.1}$$

for which the equilibrium constant, k_{eq}, is

$$k_{eq} = p*[CO]^2 /p*[O_2] = \exp(- \Delta G^o/RT), \tag{3.2}$$

in which ΔG^o is the standard Gibbs free energy change for the equilibrium. Elements in their standard states, in this case C and O_2, are defined to have a Gibbs free energy of formation, ΔG^o_f, of zero and it is also assumed throughout that the condensed phases have unit activity. Here JANAF data (ref. st71) at 1000 and 1500 K were fitted to give

$$\Delta G^o_f (CO) (cal/mol) = - 27,095 - 20.764T. \tag{3.3}$$

In general, $\Delta G^o_f = \Delta H^o_f - T\Delta S^o_f$, in which ΔH^o_f and ΔS^o_f are, respectively, the standard enthalpy and entropy of formation of, in this case, CO from the elements in this temperature range. It follows that the above entropy term is positive, but will be seen to be negative for most of the equilibria to be considered here. A rearrangement of the k_{eq} expression leads to

$$RT\ln(p*[O_2]) (cal/mol) = 2 RT\ln(p*[CO]) + 2 \Delta G^o_f(CO) \tag{3.4}$$

$$RT\ln(p*[O_2]) (cal/mol) = 2 RT\ln(p*[CO]) - 54,190 - 41.528T. \tag{3.5}$$

3

This relationship was used to calculate the oxygen potentials at several CO pressures in the Ellingham diagrams of this report. The lower temperature limit for the isobars for CO is at a CO/CO_2 of unity; at lower temperatures CO_2 is dominant and its isobars have a different slope.

4. THE Am-O-C SYSTEM

4.1 THE CONDENSED OXIDE PHASES

The Ellingham diagram for the Am-O-C system can be calculated from the data of Cordfunke et al. (ref. co90), who provide a recent critical assessment of the thermodynamics and phase behavior of the Am-O system as well as for other systems. This reference is deemed especially valid because Cordfunke and coauthors Potter and Rand have a long and excellent reputation for assessment and applications of thermodynamic data. (See note accompanying ref. co90.) They provide thermodynamic data for Am metal (solid and liquid), Am gas, Am_2O_3 and AmO_2; as they note, much of the heat capacity data have been estimated for all these phases.

Consider first the equilibrium between the metal and the sesquioxide, namely,

$$4/3 \; Am(s,l) + O_2 = 2/3 \; Am_2O_3 \tag{4.1}$$

for which the equilibrium constant, k_{eq}, is

$$k_{eq} = 1/p*[O_2] = \exp(- \Delta G^o/RT), \tag{4.2}$$

For Am_2O_3, the 1000 and 2000 K data of ref. co90 were fitted to give

$$\Delta G^o_f \; (Am_2O_3) \; (cal/mol) = - 396{,}618 + 50.93 \; T \tag{4.3}$$

Therefore, for the above equilibrium ΔG^o is $2/3 \; \Delta G^o_f \; (Am_2O_3)$ and

$$RT\ln(p*[O_2]) \; (cal/mol) = \Delta G^o = - 264{,}412 + 33.95T. \tag{4.4}$$

Similarly, for the sesquioxide-dioxide equilibrium

$$2 \; Am_2O_3 + O_2 = 4 \; AmO_2 \tag{4.5}$$
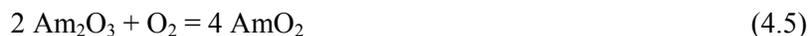
and with the 800 and 1300 K data from ref. co90, one obtains

$$\Delta G^o_f \; (AmO_2) \; (cal/mol) = - 220{,}030 + 41.41T \tag{4.6}$$

and

$$RT\ln(p*[O_2]) \; (cal/mol) = \Delta G^o = 4 \; \Delta G^o_f \; (AmO_2) - 2 \; \Delta G^o_f \; (Am_2O_3) \tag{4.7}$$

$$= - 91{,}347 + 70.62T.$$

The two oxygen potentials are shown graphically in Fig. 1.

Consider next the decomposition of AmO_2 to Am_2O_3. At $p^*[O_2]$ of one atmosphere, the above equation gives a decomposition temperature of 91,347/70.62 or 1293 K. Reference oz73 cites earlier work that states that the dioxide decomposes completely at 1673 K, but this may be the decomposition of AmO_{2-x} proposed in ref. co90 from analogy with the Ce-O and Pu-O systems. Equation 1 of ref. oz73 would give 25,250/7.985 or 3162 K for the decomposition of AmO_{2-x} and obviously there is an error in their thermochemical derivations. For the present purpose, it is sufficient to note that AmO_2 decomposes to Am_2O_3 at oxygen potentials much more positive than those for the CeO_{2-c} and PuO_{2-x} systems. This can be demonstrated by calculating the corresponding sesquioxide-dioxide reaction (not an equilibrium) from the data given in Pankratz (ref. pa82). At 1000 K the oxygen potentials for the Ce and Pu systems are -119.9 and -150.7 kcal/mol, respectively, while that for the Am system is -20.7 kcal/mol. Therefore, Am_2O_3 is the only solid oxide phase of interest to fuel kernel behavior.

4.2 THE GAS PHASES Am, AmO AND AmO$_2$

The partial pressures of Am,g, AmO,g and AmO_2,g are considered next. Reference co90 notes that americium melts at 1448 K and separate ΔG^o equations for Am,g must be used on either side of melting. For solid Am the 1000 and 1400 K data from ref. co90 give for the equilibrium Am,s = Am,g

$$\Delta G^o_f \text{ (Am,g) (cal/mol)} = 65,345 - 29.88T, \text{ T} < 1448 \text{ K} \tag{4.8}$$

and the equilibrium constant is manipulated to give

$$\log(p^*[\text{Am,g}]) = -14,282/T + 6.53, \text{ T} < 1448 \text{ K}. \tag{4.9}$$

Similarly, the 1500 and 2000 K data give

$$\Delta G^o_f \text{ (Am,g) (cal/mol)} = 58,076 - 24.86T, \text{ T} > 1448 \text{ K} \tag{4.10}$$

$$\log(p^*[\text{Am,g}]) = -12,693/T + 5.43, \text{ T} > 1448 \text{ K}. \tag{4.11}$$

These equations were used to calculate the temperatures at $\log(p^*[\text{Am}])$ of -6, -5, -4, -3, -2, -1 and zero to give 1140, 1238, 1356, 1505, 1708, 1973 and 2337 K and are shown in Fig. 1.

Further construction of the Am-O Ellingham diagram requires definition of the boundary where $p^*[\text{Am,g}] = p^*[\text{AmO,g}]$. First we estimated that

$$\Delta G^o_f \text{ (AmO,g) (cal/mol)} = -14,000 - 20.26T. \tag{4.12}$$

This estimation resulted from examination of all the lanthanide and actinide data for MO gases in ref. pe83 and the electron configurations of these elements, with the electron configurations indicative of the similarities and differences in the thermodynamics. In particular, Sm and Pu have the same electron configuration in the outer two shells and nearly identical thermodynamics for the MO gases. Since Eu and Am have identical outer electron configurations, it was assumed that the 298 K enthalpy of formation ($\Delta H^o_{f, 298}$) of AmO was identical to that for EuO at -14,000 cal/mol. The 298 K entropy values of actinide MO gases are extremely similar (ref. pe83) and it was assumed that the 298 K entropy for AmO is equal to that for PuO (58.096 cal mol^{-1} K^{-1}) and with the entropy for Am,s and O_2 (refs. co90, ja71) one obtains the above expression for ΔG^o_f (AmO,g). For the equilibrium

$$2 \text{ Am,g} + O_2 = 2 \text{ AmO,g} \tag{4.13}$$

5

and the values for Am,g at T > 1448, the equilibrium constant and oxygen potential are, respectively,

$$k_{eq} = p*[AmO]^2 /(p*[O_2] \, p*[Am]^2) \qquad (4.14)$$

$$= \exp(- (2 \, \Delta G^o_f \, (AmO,g) - 2 \, \Delta G^o_f \, (Am,g))/RT)$$

$$RTln(p*[O_2]) \, (cal/mol) = 2RTln(p*[AmO] / p*[Am]) - 144{,}200 + 9.22T. \qquad (4.15)$$

When the pressures of Am,g and AmO,g are equal the first term is zero and the oxygen potential calculated from the last two terms is plotted on Fig. 1; below that line Am,g is dominant and above the line AmO,g is dominant.

The isobars for Am,g and AmO,g in equilibrium with Am_2O_3 were calculated next and plotted on Fig. 1. In the region where Am,g is dominant, the relevant equilibrium is

$$4/3 \; Am,g + O_2 = 2/3 \; Am_2O_3 \qquad (4.16)$$

and

$$RTln(p*[O_2]) \, (cal/mol) = - 4/3 \; RTln(p*[Am,g]) + 2/3 \, \Delta G^o_f \, (Am_2O_3) - 4/3 \, \Delta G^o_f \, (Am,g) \qquad (4.17)$$

$$RTln(p*[O_2]) \, (cal/mol) = - 4/3 \; RTln(p*[Am,g]) - 351{,}509 + 73.78T, \; T < 1448 \; K \qquad (4.18)$$

$$RTln(p*[O_2]) \, (cal/mol) = - 4/3 \; RTln(p*[Am,g]) - 341{,}880 + 67.10T, \; T > 1448 \; K \qquad (4.19)$$

In the region where AmO,g is dominant, the relevant equilibrium is

$$4 \; AmO,g + O_2 = 2 \; Am_2O_3 \qquad (4.20)$$

and

$$RTln(p*[O_2]) \, (cal/mol) = - 4 \; RTln(p*[AmO,g]) + 2 \, \Delta G^o_f \, (Am_2O_3,s) - 4 \, \Delta G^o_f \, (AmO,g) \qquad (4.21)$$

$$RTln(p*[O_2]) \, (cal/mol) = - 4 \; RTln(p*[AmO,g]) - 737{,}236 + 182.9T. \qquad (4.22)$$

Further calculations require estimation of the value for ΔG^o_f (AmO$_2$,g). This is an uncertain process but two expressions were determined. The simplest was to assume ΔG^o_f (AmO$_2$,g) = ΔG^o_f (PuO$_2$,g) = -112,600 + 6.6T cal/mol from ref. ac74. A second consideration was based on the 298 K enthalpy of reaction, $\Delta H^o_{rx,298}$, data for MO$_2$,g = M,g + 2 O,g determined by Brewer and Rosenblatt, ref. br61, for several elements in the periods and groups of the periodic table. Brewer and Rosenblatt did not give data for PuO$_2$,g and thus a value of $\Delta H^o_{f,298}$ of -102,290 cal/mol for PuO$_2$,g was determined from ΔG^o_f (PuO$_2$,g) (cal/mol) = -112,600 + 6.6 T from ref. ak74 at 1500 K and the 1500 K free energy functions for the equilibrium Pu + O$_2$,g = PuO$_2$,g. This value was used to determine $\Delta H^o_{rx,298}$ = 305 kcal/mol for the reaction PuO$_2$,g = Pu,g + 2 O,g. Brewer and Rosenblatt gave $\Delta H^o_{rx,298}$ = 25520 kcal/mol for the equivalent reaction for OsO$_2$,g and the difference of 50 kcal/mol between OsO$_2$,g and PuO$_2$,g (Os lies above Pu in the periodic table) was assumed here to be the same between IrO$_2$,g (235 ± 15 kcal/mol) and AmO$_2$,g (Ir lies above Am in the periodic table). This led to $\Delta H^o_{rx,298}$ = 285 kcal/mol for the reaction AmO$_2$,g = Am,g +
2 O,g. From this value and the data for Am,g and O,g, (refs. co90, st71) one obtains $\Delta H^o_{f,298}$ (AmO$_2$,g) = -98,000 cal/mol. This value and the free energy functions for Am,g, O$_2$,g and AmO$_2$,g (using those for UO$_2$,g in the latter case) were used to calculate ΔG^o_f (AmO$_2$,g) at 1000, 1500, and 2000 K. Finally, fitting this data gave

$$\Delta G^o_f \, (AmO_2,g) \, (cal/mol) = - 98{,}000 - 2.32T. \qquad (4.23)$$

Either of these two routes to an expression for ΔG^o_f (AmO$_2$,g) probably has considerable uncertainty and the latter equation was arbitrarily chosen.

The area of the Am-O Ellingham diagram where AmO$_2$,g is dominant is considered next. For the boundary where AmO,g and AmO$_2$,g are equal, the relevant equilibrium and oxygen potential are, respectively,

$$2\ AmO,g + O_2 = 2\ AmO_2,g \tag{4.24}$$

$$RTln(p*[O_2])\ (cal/mol) = 2RTln(p*[AmO_2]\ /\ p*[AmO]) - 168,000\ + 35.88T. \tag{4.25}$$

The oxygen potentials for p*[AmO$_2$] values over Am$_2$O$_3$ were calculated from the equilibrium

$$2\ Am_2O_3 + O_2 = 4\ AmO_2,g \tag{4.26}$$

to give

$$RTln(p*[O_2])\ (cal/mol) = 4RTln(p*[AmO_2]) + 401,236 - 111.4T. \tag{4.27}$$

This equation was used to calculate the oxygen potential at several isobars of p*[AmO$_2$] in Fig. 1. These calculations give p*[AmO$_2$,g] values on the Ellingham diagram of Fig. 1 approximately 10 times higher at a given temperature and oxygen potential than those calculated from -112,600 + 6.6T cal/mol and is thus more conservative in terms of estimating americium loss during processing.

The condition for congruent evaporation of the sesquioxide can also be calculated. Lamoreaux, Hildenbrand and Brewer (ref. la87) treat this subject in detail both for a closed system and an open system, such as a Knudsen cell, and provide much data. Because the existence of the Am-O gas species was assumed, three different sets of calculations were performed, one assuming AmO$_2$ and AmO gas exist, one assuming only AmO exists, and the third with only Am gas. The congruently evaporating condition is

$$O/Am = 1.5 = (p*[AmO] + 2\ p*[AmO_2] + p*[O] + 2\ p*[O_2])/\ (p*[Am] +\ p*[AmO] + p*[AmO_2]). \tag{4.28}$$

The value of p* for each species was calculated for an equilibrium such as 4 AmO,g + O$_2$ = 2 Am$_2$O$_3$ at a given p*[O$_2$] and T in a spreadsheet and p*[O$_2$] iterated until O/Am = 1.50, and then the process was repeated at different temperatures. The conditions for congruent evaporation were calculated to be

$$RTln(p*[O_2])\ (cal/mol) = -\ 184,635 + 45.76T\ (with\ AmO_2,\ AmO\ and\ Am) \tag{4.29}$$

$$RTln(p*[O_2])\ (cal/mol) = -\ 164,051 + 37.66T\ (with\ AmO\ and\ Am). \tag{4.30}$$

$$RTln(p*[O_2])\ (cal/mol) = -\ 158,663 + 29.35T\ (with\ Am). \tag{4.31}$$

The range of oxygen potentials calculated from these equations lies approximately 10 kcal/mol on either side of the equilibrium 2 AmO,g + O$_2$ = 2 AmO$_2$,g that is plotted in Fig. 1.

Figure 1 illustrates the most conservative conditions for americium loss by evaporation at oxygen potentials more positive than -80,000 cal/mol. This results from the assumption that AmO gas and AmO$_2$ gas exist. If neither existed, or if only AmO and Am gas existed, it can be seen from the extension of their isobars that the gaseous vapor pressures would be much lower than when all three species exist. Even with all three species, ceramic processing should be possible up to 1600°C at H$_2$/H$_2$O = 1000 and still maintain all Am-O gaseous partial pressures < 10^{-8} atm. Even under this condition the worst

processing condition would be a rapid flow of the processing gas past the americium oxide, since the flowing gas would transpire the Am gaseous species. The best condition would be processing in the same atmosphere, but in a covered crucible, which would limit this transpiration.

4.3 EQUILIBRIA INVOLVING $AmC_{1.5}$

Consider next the effect of $AmC_{1.5}$ in the Am-O-C system. There is an equilibrium between carbon, the sesquioxide, and the sesquicarbide. At oxygen potentials below this equilibrium, decomposition of the sesquicarbide to carbon and Am,g will determine the Am,g partial pressure. To perform the calculations it is assumed that, in the absence of data,

$$\Delta G^o_f (AmC_{1.5}) = \Delta G^o_f (PuC_{1.5}) \text{ (cal/mol)} = - 21{,}370 + 2.06T \quad (4.32)$$

in which the numerical values come from ref. be77. The oxide-carbide equilibrium and oxygen potential are, respectively,

$$4/3 \, AmC_{1.5} + O_2 = 2 \, C + 2/3 \, Am_2O_3 \quad (4.33)$$
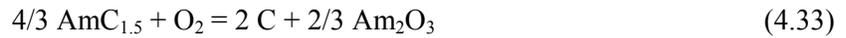
$$RT\ln(p*[O_2]) \text{ (cal/mol)} = 2/3 \, \Delta G^o_f (Am_2O_3) - 4/3 \, \Delta G^o_f (AmC_{1.5}) \quad (4.34)$$

$$RT\ln(p*[O_2]) \text{ (cal/mol)} = - 239{,}795 + 33.14T. \quad (4.35)$$

This relationship is also plotted on Fig. 1. Below this line only carbon and $AmC_{1.5}$ are present and the Am,g pressures, which are independent of the oxygen potential, can be calculated for the equilibrium

$$AmC_{1.5} = Am,g + 1.5 \, C \quad (4.36)$$

for which

$$\log(p*[Am]) = - 17{,}906/T + 6.19. \quad (4.37)$$

The temperatures at which $\log(p*[Am])$ (in atmospheres) is -6, -5, 4, -3 and -2 are 1468, 1600, 1757, 1948 and 2186 K, respectively. These are not plotted in Fig. 1, but can be obtained by dropping a vertical line from the sesquioxide-sesquicarbide equilibrium at its intersection with a particular Am,g isobar.

Of greater consequence for the transmutation fuel is the probability that an oxycarbide kernel cannot be synthesized by carbothermic conversion of an oxide-carbide mixture. To demonstrate this, consider the equilibrium and equilibrium constant, respectively,

$$1/3 \, Am_2O_3 + 3.5 \, C + Am,g = 5/3 \, AmC_{1.5} + CO \quad (4.38)$$

$$k_{eq} = p*[CO]/p*[Am,g] \quad (4.39)$$

$$= \exp(- [5/3 \, \Delta G^o_f (AmC_{1.5}) + \Delta G^o_f (CO) - \Delta G^o_f (Am,g) - 1/3 \, \Delta G^o_f (Am_2O_3)]/RT)$$

$$= \exp(- 5{,}230/T + 4.36).$$

At the usual carbothermic conversion temperatures of ~ 1800 K the ratio is ~ 4. Since carbothermic conversion requires removal of CO by flowing gas or in a vacuum, it is clear that Am,g would also be removed at an unacceptable rate. This CO-Am,g relationship can also be seen graphically in Fig. 1 at the sesquioxide-sesquicarbide equilibrium since the isobars for Am,g and CO have similar values.

4.4 EQUILIBRIA INVOLVING AmN

The compound AmN is not involved in the transmutation fuel but is considered here in the broader context of understanding the volatility of Am-containing systems. Ogawa et. al. (ref. og95) measured Pu,g and Am,g partial pressures over a (Pu,Am)N specimen containing 0.0027 mol % AmN. Their data permitted their determination of $\Delta H^o_{f,298}$ (AmN) = -70.27 kcal/mol, which compared very closely to the values they referenced for UN (-70.7 kcal/mol), PuN (-71.5 kcal/mol) and LaN (-71.9 kcal/mol). In general, they estimated from PuN and UN data that for pure AmN

$$\Delta G^o_f \text{ (AmN) (cal/mol)} = - 71,140 + 22.0T \tag{4.40}$$

for the equilibrium Am,s + 0.5 N_2 = AmN. They also determined the condition for vaporization in their experiments, where they derived p*[Am,g] = 5.84p*[N_2], which for the equilibrium and equilibrium constant are, respectively,

$$AmN = Am,g + 0.5 \ N_2 \tag{4.41}$$

$$k_{eq} = p^*[N_2]^{0.5}p^*[Am,g] \tag{4.42}$$

which lead to

$$p^*[Am,g] = 1.81 \ exp(- 45,590/T + 17.21). \tag{4.43}$$

The temperatures where log(p*[Am,g]) is -6, -4, -2 and zero are 1442, 1688, 2035 and 2561 K, respectively. The equilibrium for p*[N_2] = 1, where the factor 5.84 is not relevant, leads to

$$log(p^*[Am,g]) = - 28,505/T + 10.43 \tag{4.44}$$

and at log(p*[Am,g]) of –8, -6, -4 and -2 the temperatures are 1562, 1753, 1996, 2317 K, respectively.

4.5 GENERAL COMMENTS ON AMERICIUM VOLATILITY

It is clear that americium-containing systems can have partial pressures of Am,g, AmO,g and AmO_2,g that can lead to americium loss at the usual temperatures for ceramic processing, but, under some conditions, the volatility is low enough to permit processing. Figure 1 for the Am-O system clearly shows appreciable Am-containing gases at very reducing conditions but, on the other hand, from an atmosphere of air down to usefully reducing conditions (H_2/H_2O = 1000), Fig. 1 illustrates that temperatures < 1900 K can probably be used because log(p*[Am,g]) < - 8. The calculations in Sect. 4.3 indicate that carbothermic processing to make an oxycarbide in the Pu-Am-C-O system would be improbable because the pressures of CO and Am,g are similar and one cannot remove the CO from carbothermic conversion without removing substantial Am. In the case of AmN, Ogawa et. al. (ref. og95) note, "a high nitrogen pressure…suppressed the evaporative loss of americium" and the calculations in Sect. 4.4 demonstrate that one atmosphere of nitrogen can permit processing of AmN to 1562–1753 K. Obviously the processing of metallic fuels is the worst case, as demonstrated by Trybus et. al. (ref. tr93). They processed U-Pu-Zr fuels containing 2.1% Am at 1738 K, where they realized p*[Am,g] = 0.003 atm from ref co90, and lost 40% of the Am in spite of taking measures to minimize Am loss.

5. THE Pu-O-C SYSTEM

5.1 THE CONDENSED PHASES

At reactor temperatures, the relevant oxide phases are Pu_2O_3 and PuO_{2-x} with $0 < x < 0.4$ (refs. be87, be86, sa68) and the carbide in equilibrium with carbon is $PuC_{1.5}$. Thermodynamic data will be taken from ref. be77, which collected well-established data available at that time. Since the Pu-O system has been studied to a much greater degree than the Am-O system and its characteristics are better understood, the Pu-O Ellingham diagram of Fig. 2 will be developed more succinctly, but using methodology identical to that for the Am-O-C system. For the $Pu-Pu_2O_3-O_2$ equilibrium

$$\Delta G^o_f (Pu_2O_3) \ (cal/mol) = -\ 399{,}600 + 63.8T \tag{5.1}$$

$$RT\ln(p^*[O_2]) \ (cal/mol) = 2/3 \ \Delta G^o_f (Pu_2O_3) = -\ 266{,}400 + 42.53T. \tag{5.2}$$

For the equilibrium $4/3 \ PuC_{1.5} + O_2 = 2 \ C + 2/3 \ Pu_2O_3$

$$RT\ln(p^*[O_2]) \ (cal/mol) = 2/3 \ \Delta G^o_f (Pu_2O_3) - 4/3 \ \Delta G^o_f (PuC_{1.5}) \tag{5.3}$$

$$RT\ln(p^*[O_2]) \ (cal/mol) = -\ 237{,}907 + 39.78T. \tag{5.4}$$

The behavior of the PuO_{2-x} phase and its solution with urania was modeled in ref. be85 and applied to all literature $p^*[O_2]$-x data, which, in the case of pure plutonia, had 418 data values over the ranges $\sim 950 < T < 1800$ K and $0.001 < x < \sim 0.36$. The slight corrections to the model that appear in refs. be83 and be87 have insignificant effects on the performance of reactor fuels. The model for PuO_{2-x} in ref. be86 that attempted to improve that in ref. be85 should not be used because the non-ideal term goes through a minimum at $x \cong 0.28$ and thus poorly represents the data above $x = 0.24$; the non-ideal term $(3 - 12x\ldots,$ below$)$ of the original model exhibits only slight curvature over the range of x and thus represents the data well. The model of ref. be85 gives

$$RT\ln(p^*[O_2]) \ (cal/mol) = -\ 196{,}000 + 40.26 \ T \tag{5.5}$$

$$-\ 3RT\ln(\ 1.5x(1 - 0.5x)^{1/3} / [1-2x]^{4/3} \ )$$

$$-\ (13{,}184 - 11.8T)(3 - 12x + 3x^2)/(1 - 0.5x)^2.$$

This relationship was used at specific x values to give

$$RT\ln(p^*[O_2]) \ (cal/mol) = -\ 239{,}912 + 99.28T, \ x = 0.01 \tag{5.6}$$

$$RT\ln(p^*[O_2]) \ (cal/mol) = -\ 234{,}650 + 84.80T, \ x = 0.05 \tag{5.7}$$

$$RT\ln(p^*[O_2]) \ (cal/mol) = -\ 226{,}990 + 73.83T, \ x = 0.10 \tag{5.8}$$

$$RT\ln(p^*[O_2]) \ (cal/mol) = -\ 218{,}690 + 63.95T, \ x = 0.15 \tag{5.9}$$

$$RT\ln(p^*[O_2]) \ (cal/mol) = -\ 209{,}710 + 54.08T, \ x = 0.20 \tag{5.10}$$

$$RT\ln(p^*[O_2]) \ (cal/mol) = -\ 199{,}900 + 43.78T, \ x = 0.25 \tag{5.11}$$

$$RT\ln(p^*[O_2]) \text{ (cal/mol)} = -189,240 + 32.62T, \; x = 0.30 \qquad (5.12)$$

$$RT\ln(p^*[O_2]) \text{ (cal/mol)} = -177,660 + 20.48T, \; x = 0.35 \qquad (5.13)$$

$$RT\ln(p^*[O_2]) \text{ (cal/mol)} = -164,938 + 6.63T, \;\; x = 0.40. \qquad (5.14)$$

These were used to plot the oxygen potentials at the given 2-x values in Fig. 2.

5.2 THE GAS PHASES Pu, PuO AND PuO$_2$

The oxygen potential boundary where $p^*[Pu,g]$ equals $p^*[PuO,g]$ is calculated from the equilibrium

$$2\,Pu,g + O_2 = 2\,PuO,g \qquad (5.15)$$

and with the values (ref. be77)

$$\Delta G^o_f \text{ (PuO,g) (cal/mol)} = -28,500 - 9.7T \qquad (5.16)$$

$$\Delta G^o_f \text{ (Pu,g) (cal/mol)} = 78,110 - 21.23T, \; T > 913 \text{ K} \qquad (5.17)$$

the equilibrium constant and oxygen potential are, respectively,

$$k_{eq} = p^*[PuO]^2/(p^*[O_2]\,p^*[Pu]^2) = \exp(-2\,[\Delta G^o_f \text{ (PuO,g)} - \Delta G^o_f \text{ (Pu,g)}]/RT), \qquad (5.18)$$

$$RT\ln(p^*[O_2]) \text{ (cal/mol)} = 2RT\ln(\,p^*[PuO]\,/\,p^*[Pu]) - 213,220 + 23.06T. \qquad (5.19)$$

Plutonium melts at 913 K and thus ΔG^o_f (Pu,g) given here is referenced to the liquid. When the pressures are equal the first term is zero and the oxygen potential calculated from the last two terms is plotted on Fig. 2; below that line Pu,g is dominant and above the line PuO,g is dominant.

Similarly, the boundary where $p^*[PuO,g]$ equals $p^*[PuO_2,g]$ is calculated from the equilibrium

$$2\,PuO,g + O_2 = 2\,PuO_2,g \qquad (5.20)$$

and with the value (ref. ac74)

$$\Delta G^o_f \text{ (PuO}_2\text{,g) (cal/mol)} = -112,600 + 6.6T \qquad (5.21)$$

$$RT\ln(p^*[O_2]) \text{ (cal/mol)} = 2RT\ln(\,p^*[PuO_2]\,/\,p^*[PuO]) - 168,200 + 32.6T. \qquad (5.22)$$

The isobars for Pu,g, PuO,g and PuO$_2$,g were calculated next and plotted on Fig. 2. In the region where Pu,g is dominant, over Pu$_2$O$_3$ the relevant equilibrium and oxygen potential are, respectively,

$$4/3\,Pu,g + O_2 = 2/3\,Pu_2O_3 \qquad (5.23)$$

$$RT\ln(p^*[O_2]) \text{ (cal/mol)} = -4/3\,RT\ln(p^*[Pu,g]) + 2/3\,\Delta G^o_f \text{ (Pu}_2\text{O}_3\text{)} - 4/3\,\Delta G^o_f \text{ (Pu,g)} \qquad (5.24)$$

$$RT\ln(p^*[O_2]) \text{ (cal/mol)} = -4/3\,RT\ln(p^*[Pu,g]) - 370,550 + 70.84T. \qquad (5.25)$$
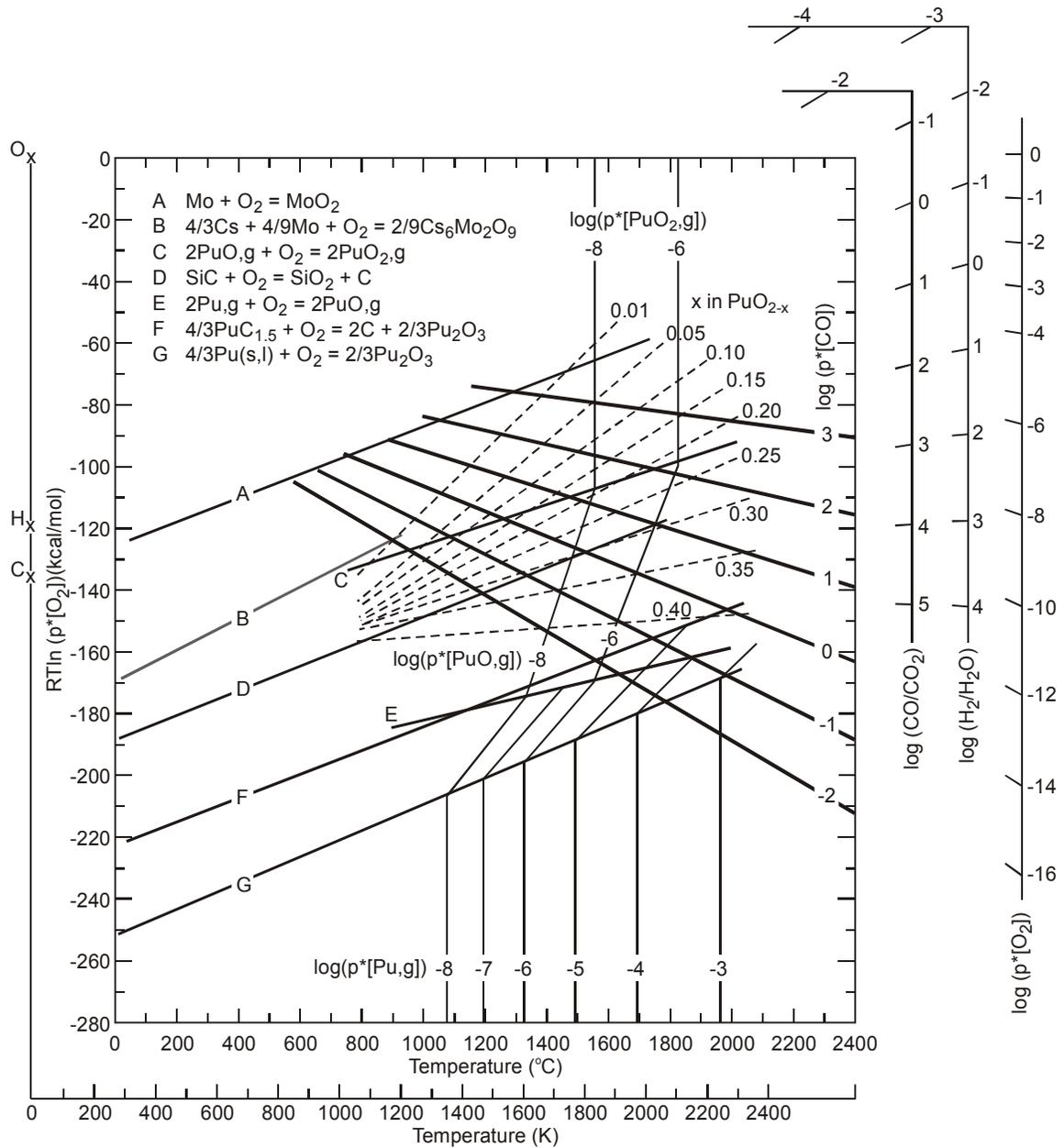
Fig. 2. The Ellingham diagram for the Pu-O-C fuel system. (The oxygen potentials for the Pu,g-PuO,g and PuO,g-PuO₂,g equilibria are plotted where the two pressures in each equilibrium are equal.)

In the region where PuO,g is dominant, over the phase regions containing Pu_2O_3 the relevant equilibrium and oxygen potential are, respectively

$$4 \text{ PuO,g} + O_2 = 2 \text{ Pu}_2O_3 \qquad (5.26)$$

$$RT\ln(p^*[O_2]) \text{ (cal/mol)} = -4 RT\ln(p^*[\text{PuO,g}]) + 2 \Delta G^o_f (\text{Pu}_2O_3,s) - 4 \Delta G^o_f (\text{PuO,g}) \qquad (5.27)$$

$$RT\ln(p^*[O_2]) \text{ (cal/mol)} = -4 RT\ln(p^*[\text{PuO,g}]) - 685,200 + 166.4T. \qquad (5.28)$$

In the region where PuO_2,g is dominant, the relevant equilibrium is

$$PuO_2 = PuO_2,g \qquad (5.29)$$

and with (ref. be85, from ref. pa82)

$$\Delta G^o_f (\text{PuO}_2) \text{ (cal/mol)} = -250,430 + 44.86T \qquad (5.30)$$

one obtains

$$p^*[\text{PuO}_2,g] = \exp([-137,830 + 38.26T]/RT) \text{ or} \qquad (5.31)$$

$$\log (p^*[\text{PuO}_2]) = -30,125/T + 8.36. \qquad (5.32)$$

At $\log (p^*[\text{PuO}_2])$ values of -12, -10, -8, -6, -4, and -2, the latter equation leads to temperatures of 1480, 1641, 1841, 2098, 2437 and 2907 K, respectively. These isobars are plotted in Fig. 2.

The treatment of the equivalent Cm-O system is beyond the scope of the present work, but examination of the limited thermodynamic data indicates behavior of the gaseous species similar to that of the Pu-O system.

Consider next Pu,g and PuO,g during the carbothermic conversion of an oxide-carbide mixture. Means to control plutonium losses have been studied in great detail (refs. be77, ri78) and the reader is referred to that work. Some of the general factors that affect the process are shown in Fig. 2. It illustrates that PuO,g is slightly dominant relative to Pu,g over the Pu_2O_3-$PuC_{1.5}$-C mixture and Fig. 2 of ref. be77 illustrates that the CO/(PuO + Pu) value is about 10,000. On the other hand, if the process reaches the Pu_2O_3-$PuC_{1.5}$-Pu(C,O) phase field, the ratio is ~ 10 and significant plutonium losses could occur. Another factor affecting oxide-to-carbide conversion is the absolute pressure of Pu-containing gases; at the usual temperatures of about 1400 to 1700°C Fig. 2 illustrates that $p^*[\text{PuO}] < 10^{-6}$ at the Pu_2O_3-$PuC_{1.5}$-C equilibrium, a pressure that is low enough to permit minimization of plutonium loss.

Also note that the pressure isobars shown in Fig. 2 below the oxide-carbide equilibrium are those over the oxide system in the absence of the carbide. [Some of the thermodynamic values from ref. be77 originated from publications from Argonne National Laboratory (ANL). After the present paper was finished, the present author found subsequent ANL publications (refs. gr83, gr82, gr80a, gr80b) that give slightly different thermodynamic values. In addition, the U-O and Th-O systems were analyzed. Data in the newer ANL references should be used for future work, but the differences have only slight effects on the calculations, figures, and conclusions presented here, and thus the present author continued to use the data in ref. be77.]

6. HYDROGEN REDUCTION OF PuO$_{2-x}$

The quantitative model of Sect. 5.1 is used here to recalculate the parameters of ref. li71 that permit control of the process for hydrogen or C-CO reduction of PuO$_{2-x}$. Equation 3 of ref. li71 calculates the increment of time, Δt, needed to reduce the plutonia and is restated here as

$$\Delta t = 22.415 \ N \ H \ \Delta x / f[H_2] \qquad (6.1)$$

in which N is the moles of PuO$_{2-x}$ being reduced, H is the average H$_2$/H$_2$O ratio over Δx, and f[H$_2$] is the flow of hydrogen in liters (STP) per unit time. Since the H$_2$/H$_2$O ratio is a function of the oxygen potential,

$$RTln(p*[O_2]) \ (cal/mol) = 2 \ RTln(p*[H_2O/H_2]) + 2 \ \Delta G^o_f \ (H_2O). \qquad (6.2)$$

The JANAF data (ref. st71) at 1000 and 2000K gives ΔG^o_f(H$_2$O) (cal/mol) = -59,679 + 13.64T. Upon equating the oxygen potential here with the oxygen potential equation for plutonia in Sect. 5.1 and rearranging the terms one obtains

$$H_2/H_2O = exp[\ 19,342/T - 3.27 + 1.5ln(\ 1.5x(1 - 0.5x)^{1/3} / (1 - 2x)^{4/3} \ ) \qquad (6.3)$$
$$+ (3,817/T - 2.97)(3 - 12x + 3x^2)/(1 - 0.5x)^2 \ ].$$

Here the parameter H was calculated in increments of 0.01 for Δx from x = 0.01 to x = 0.4. At approximately x = 0.4 or O/Pu = 1.6, H$_2$/H$_2$O remains constant across the two-phase region PuO$_{1.5}$-PuO$_{1.6}$ and the continuation of reduction to O/Pu = 1.5 can also be calculated across Δx = 0.1. The value of H was summed (essentially integrated) over $0.01 \leq x \leq 0.50$ in a spreadsheet at a given temperature and the results, which are $\int (H_2/H_2O) \ dx$, are shown in Fig. 3 at specific values of x. The values shown in Fig. 3 are also the number of moles of H$_2$ needed to reduce one mole of PuO$_2$ to a given x value at a given temperature. (Note that the integral shown in Fig. 2 of ref. li71 is not directly comparable to the present integral because the former is evaluated in increments of the valence of plutonium, i.e., twice the increment in x.) The time to attain a given value of x is then

$$t = 22.415 \ N \int (H_2/H_2O) \ dx/f[H_2]. \qquad (6.4)$$

For example, a reasonable flow past one mole or ~ 40 cm^3 of loosely packed plutonia would be f[H$_2$] = 2.24 l/min; at 1900 K it would take 1000 min (16.6 h) and 100,000 min (167 h), respectively, to reduce one mole of PuO$_2$ to PuO$_{1.7}$ and PuO$_{1.5}$. Use of Ar-4%H$_2$ would increase these times by a factor of 25 at the same flow rate. The C-CO-CO$_2$ system can also be used to reduce plutonia in times shorter than those for hydrogen reduction and the reader is referred to ref. li71 for details.

The integration in Fig. 3 is considerably different from that given in Fig. 2 of ref. li71 and is a consequence of having a much better representation of the plutonia data. Use of the data of Fig. 3 at 1800 K, a reasonable temperature for reduction, would predict reduction times shorter by a factor of ~ 0.1 for $x \leq 0.2$, approximately equal times at x = 0.25, and times longer by a factor of ~ 5 at $x \geq 0.4$. Reference li71 lists results from several reductions and the predicted time for reduction was about a factor of five greater than the actual time needed to accomplish a given O/Pu. Use of the integration of Fig. 3 would reduce this factor to about two, which appears to be very good agreement. One variable that reduced the times even more appeared to be the residual carbon in the plutonia prior to hydrogen reduction. Therefore, it would appear that present-day experiments with the plutonia-containing kernels of the driver and transmutation fuels are needed to calibrate the hydrogen-reduction process.
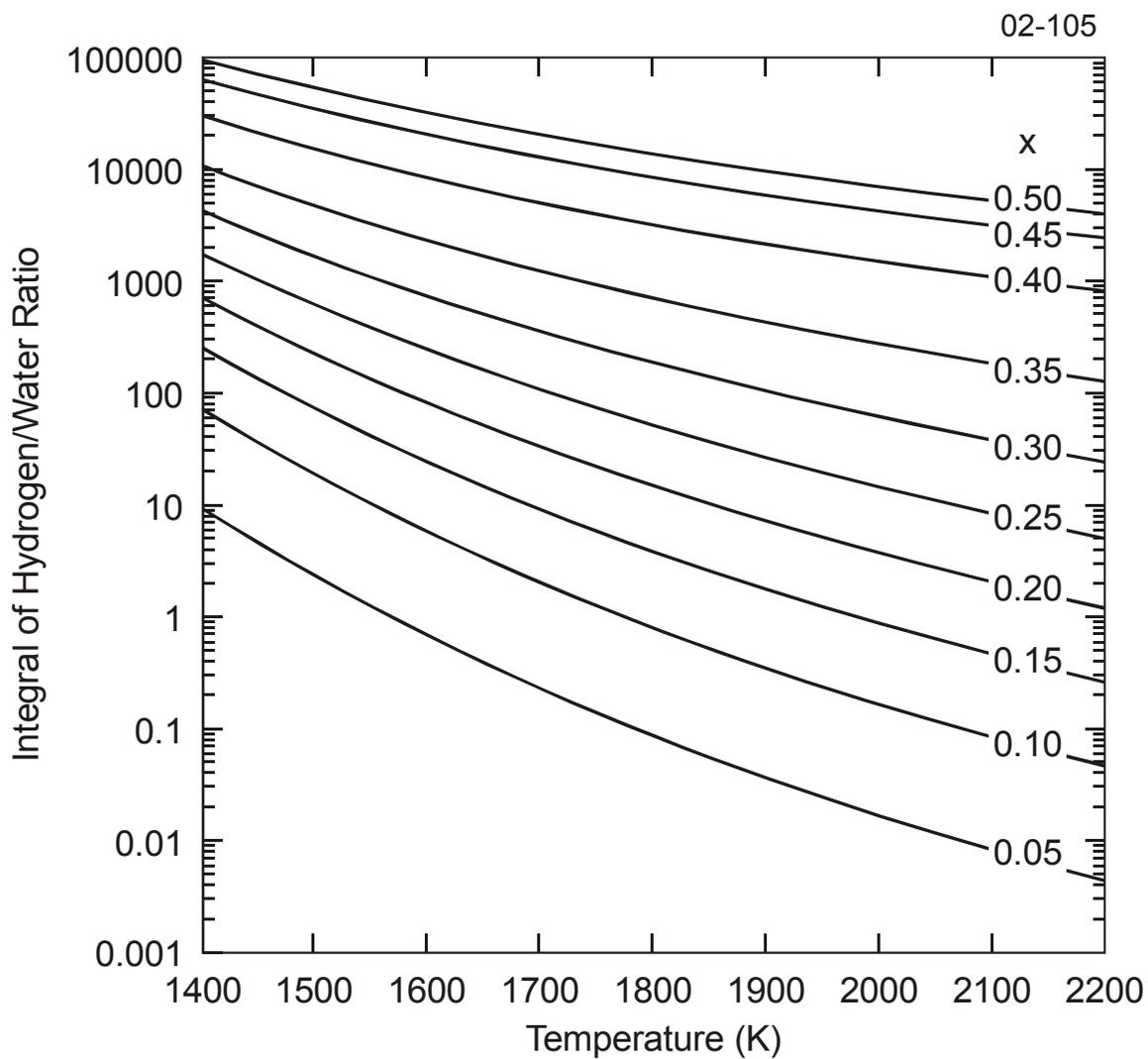
Fig. 3. Equilibrium-limited factor, I[H], for reduction of PuO$_{2-x}$. (Integration of H$_2$/H$_2$O from x = 0.01 to x = 0.50 for the PuO$_{2-x}$ phase and the PuO$_{1.6}$-PuO$_{1.5}$ two-phase region. The numerical values are also the moles of hydrogen needed to reduce PuO$_{1.99}$ to a given O/Pu.

The integration in Fig. 3 can also be represented mathematically at given x values. Upon defining $I[H] = \int (H_2/H_2O) \, dx$, one obtains

$$Log(I[H]) = 12{,}790/T - 8.16, \, x = 0.05 \tag{6.5}$$

$$Log(I[H]) = 12{,}129/T - 6.83, \, x = 0.10 \tag{6.6}$$

$$Log(I[H]) = 11{,}412/T - 5.76, \, x = 0.15 \tag{6.7}$$

$$Log(I[H]) = 10{,}573/T - 4.72, \, x = 0.20 \tag{6.8}$$

$$Log(I[H]) = 9{,}623/T - 3.65, \, x = 0.25 \tag{6.9}$$

$$Log(I[H]) = 8{,}540/T - 2.50, \, x = 0.30 \tag{6.10}$$

$$Log(I[H]) = 7{,}305/T - 1.22, \, x = 0.35 \tag{6.11}$$

$$Log(I[H]) = 5{,}886/T + 0.23, \, x = 0.40 \tag{6.12}$$

$$Log(I[H]) = 5{,}325/T + 0.97, \, x = 0.45 \tag{6.13}$$

$$Log(I[H]) = 5{,}194/T + 1.25, \, x = 0.50 \tag{6.14}$$

7. OXYGEN RELEASE DURING FISSION

It is well known that only part of the oxygen released during fission of actinide oxides is combined with very stable oxides. The latter are zirconia, strontia, baria, yttria and the lanthanide oxides. In the gas-cooled reactor fuel particle, a portion of the released oxygen combines with carbon to form CO and, at low temperatures, CO_2. The primary consideration to fuel design is the pressure-vessel contribution of CO to the hoop stresses in the particle coatings. An indirect effect is the establishment of oxygen potentials high enough to result in kernel migration, an effect that, if sufficient to cause fuel performance problems, is negated by means such as use of the oxycarbide kernel, or in some cases, a substoichiometric oxide kernel.

This section provides a review and discussion of the measurements of CO in terms of oxygen atoms released per fission, O/f, in ThO_2, UO_2, and their solid solution. Here f is defined as the fraction FIMA, fissions per initial actinide metal atom. These results will be compared to those predicted from experimental measurements and modeling of the behavior of CeO_{2-c} and the $U_{1-z}Gd_zO_{2-g}$ solid solution, where Gd is assumed to be a surrogate for Y and the lanthanide fission products. The latter thermodynamic data will permit, for the first time, calculation of O/f as a function of burnup, temperature, particle void volume and $p^*[O_2]$ for comparison with the experimental measurements. These calculations are far from perfect, but are probably accurate enough for particle pressure-vessel considerations and, possibly, the oxygen potential of the fuel system.   Also to be illustrated is the substantial difference between fuels containing uranium oxide and those such as the driver and transmutation fuels that do not; when urania is present the solution of lanthanide fission product oxides permits promotion of the O/U above two, and incorporation of some of the oxygen released by fission in the oxide kernel. In the case of fuel containing PuO_{2-x}, the O/Pu can be no higher than two and the oxygen released by fission can only form CO and increase the O/Pu of the remaining PuO_{2-x}, as will be demonstrated.

7.1 THE FISSION-PRODUCT YIELDS

The fission-product yields are needed to calculate the oxygen combined as very stable oxides and these have been taken from England and Rider (ref. en93) for fission at thermal neutron energies. Katcoff (ref. ka60) provides the fission-product decay chains that led to the masses of the long-lived or stable isotopes used here. The fission of ^{233}U, ^{235}U, ^{239}Pu and ^{241}Am are considered here and the percent yields are given in Table 1, which lists about 87% of the fission products.

The oxygen combined in the very stable oxide fission products per initial actinide oxide is calculated next. It is assumed that O/Zr = 2, O/(Ba + Sr) = 1, and O/(Y + Lanthanides) = 1.5. The compound CeO_{2-c} is considered to be present as $CeO_{1.5}$ in the calculation of O/f in the table below and the effects of the actual substoichiometry will be considered in subsequent sections as needed. The oxygen released per actinide fission is then taken here as the difference between the initial O/actinide and the oxygen combined in the very stable oxides, as shown in Table 1. Other fission product yields to be considered later are also given in Table 1.

Table 1. Fission product yields in percent and oxygen balance per actinide fission

Element	Mass	^{233}U	^{235}U	^{239}Pu	^{241}Am
Very stable oxide group					
Zr	91-4, 96	32.53	30.37	18.51	14.00
Sr	88, 90	12.26	9.59	3.43	2.14
Ba	138	5.91	6.75	6.12	6.93
Y	89	6.34	4.81	1.72	0.99
La	139	6.31	6.59	5.64	6.67
Ce	140, 142	13.09	12.28	10.29	10.66
Pr	141	6.48	5.87	5.25	4.79
Nd	143-6, 148, 150	18.53	20.75	16.21	16.10
Pm	147	1.74	2.26	2.00	2.03
Sm	149, 151, 152, 154	1.36	1.82	2.80	3.37
Eu	153, 155	0.12	0.19	0.53	0.91
Combined oxygen per actinide fission		1.64	1.59	1.13	1.05
Oxygen (O) released per actinide fission		0.36	0.41	0.87-x	0.45
Possible oxide formers					
Mo	95, 97, 98, 100	21.52	24.53	22.83	21.38
Cs	133, 137		13.00	13.63	11.92
Rb	77.5% of 85, 87	3.33	3.33	1.57	1.02
Non-oxide forming elements					
Pd	105, 107, 108		1.16	11.13	15.96
Rh	103		3.03	7.00	6.23
Ru	101, 102, 104		11.35	18.23	18.41
Ag	109		0.031	1.48	2.49
Kr	83, 84, 22.5% of 85, 86	3.86	3.86	1.67	0.98
Xe	131, 132, 134, 136		28.13	25.76	24.49

7.2 THE $U_{1-z}Gd_zO_{2\pm g}$, CeO_{2-c}, AND Sr-Mo-O SYSTEMS

The urania-gadolinia and ceria systems exhibit extensive oxygen nonstoichiometry and the chemical thermodynamic representations (refs. li88, li86a, li86b) for the experimental data for these systems will be used here to calculate O/f for comparison with experimental measurements. The behavior of the urania-gadolinia system is assumed to represent that of the solution of Y and the lanthanides in urania, while

ceria, which is the only fission-product lanthanide that approaches an oxygen-to-metal ratio of two, is included in the calculations because it makes a contribution to the O/f calculations that is about 10% of that for the urania-gadolinia system.

The urania-gadolinia system exhibits oxygen-to-metal values above and below two, but in the coated particle the oxygen potentials restrict the values to < 2. For substoichiometry the oxygen potential is given by eq. 23 of ref. li88 and is

$$RTln(p*[O_2]) \text{ (cal/mol)} = -180{,}115 + 470.1T + RTln(N_3^6/ N_4^3 N_1^4) \tag{7.1}$$

in which N_3, N_4 and N_1 are mole fractions of the mass parameters $U_{2/3}Gd_{2/3}O_{8/3}$, $Gd_{4/3}O_2$ and UO_2, respectively, used to model the experimental data. The compositions in this system lie between UO_2, $UGdO_4$ (i.e., 0.5 $U_2O_5*Gd_2O_3$) and Gd_2O_3 and the mass parameters are reformulations of these compositions. The moles of each are $m_3 = 1.5(z-2g)$, $m_4 = 1.5g$ and $m_1 = 1- 2z +2g$ and the mole fractions are calculated from these. It follows from m_3 that $g < 0.5 z$ and the maximum oxygen uptake beyond the minimum of the UO_2-$GdO_{1.5}$ lower limit is $0.5 z$, which is applicable for $z <= 0.5$, and from m_1 that $g > z - 0.5$ for $z > 0.5$. Unit activity of the urania-gadolinia system was assumed because calculations in $Th_{1-w}U_wO_2$ where the thoria content of the particles was included in the mole fractions, (i.e., an ideal solid solution) had little effect on the results. Figure 4 illustrates an example of the values of g and the corresponding O/U values at $z = 0.35$, which is the approximate value of z in the thoria particles studied by the author, (Sect. 7.3) at 5% FIMA and in urania particles at 50% FIMA.

The Ce-O system includes a CeO_{2-c} phase that exhibits a miscibility gap below approximately 958 K. Reference li86b reports the analysis of an extensive literature data base that led to the representation of the oxygen potential by eq. 12 of that reference by

$$RTln(p*[O_2]) \text{ (cal/mol)} = -236300 + 86.94T + 4RTln(N_{2a}) - 5RTln(N_{1a}) \tag{7.2}$$

$$+ (-16{,}781 + 7.66T) [(4 N_{1a} (1- N_{2a}) - 5 N_{2a} (1 - N_{1a})]$$

$$+ (-15{,}240 + 7.66T) [4N_{1a} \{ -2N_{2a} + N_{1a} + 2N_{2a} (N_{2a} - N_{1a})\}$$

$$- 5 N_{2a} \{2N_{1a} - N_{2a} - 2N_{1a} (N_{1a} - N_{2a})\}]$$

in which N_{1a} and N_{2a} are the mole fractions of two mass parameters $Ce_{0.8}O_{1.2}$ (a reformulation of Ce_2O_3) and CeO_2, respectively, used to model the CeO_{2-c} phase. The moles are $m_{1a} = 2.5c$ and $m_{2a} = 1 - 2c$. The expression of the last three lines is the Redlich-Kister term necessary to represent the oxygen potential data near the miscibility gap in CeO_{2-c}. The further extension of the analysis to the urania-ceria system in ref. li86a was not included since the additional complexity was not warranted because the contribution of CeO_{2-c} to the O/f calculations was only about 10% of that from the urania-gadolinia system.

Assumptions concerning inclusion of ceria in the urania-lanthanide oxide solution will be considered later.

The Sr-Mo-O system contains several double oxide compounds composed of SrO and either MoO_2 or MoO_3. The phase diagram of Fig. 5 was obtained from Lindblom and Rosen (ref. li86c), who determined the oxygen potentials shown in Fig. 4 for the Mo-SrO-Sr_2MoO_4 and $SrMoO_3$-$SrMoO_4$ phase fields. These data are possibly relevant to O/f calculations because they lower the oxygen potentials for the Mo-O system into the range that is observed at the lower operating temperatures for oxide fuels. Depending on which phase is stable, these phases could possibly combine with one to three oxygen atoms per SrO as a result of the oxidation of Mo. Consequently, these thermodynamic data will be developed fully here.
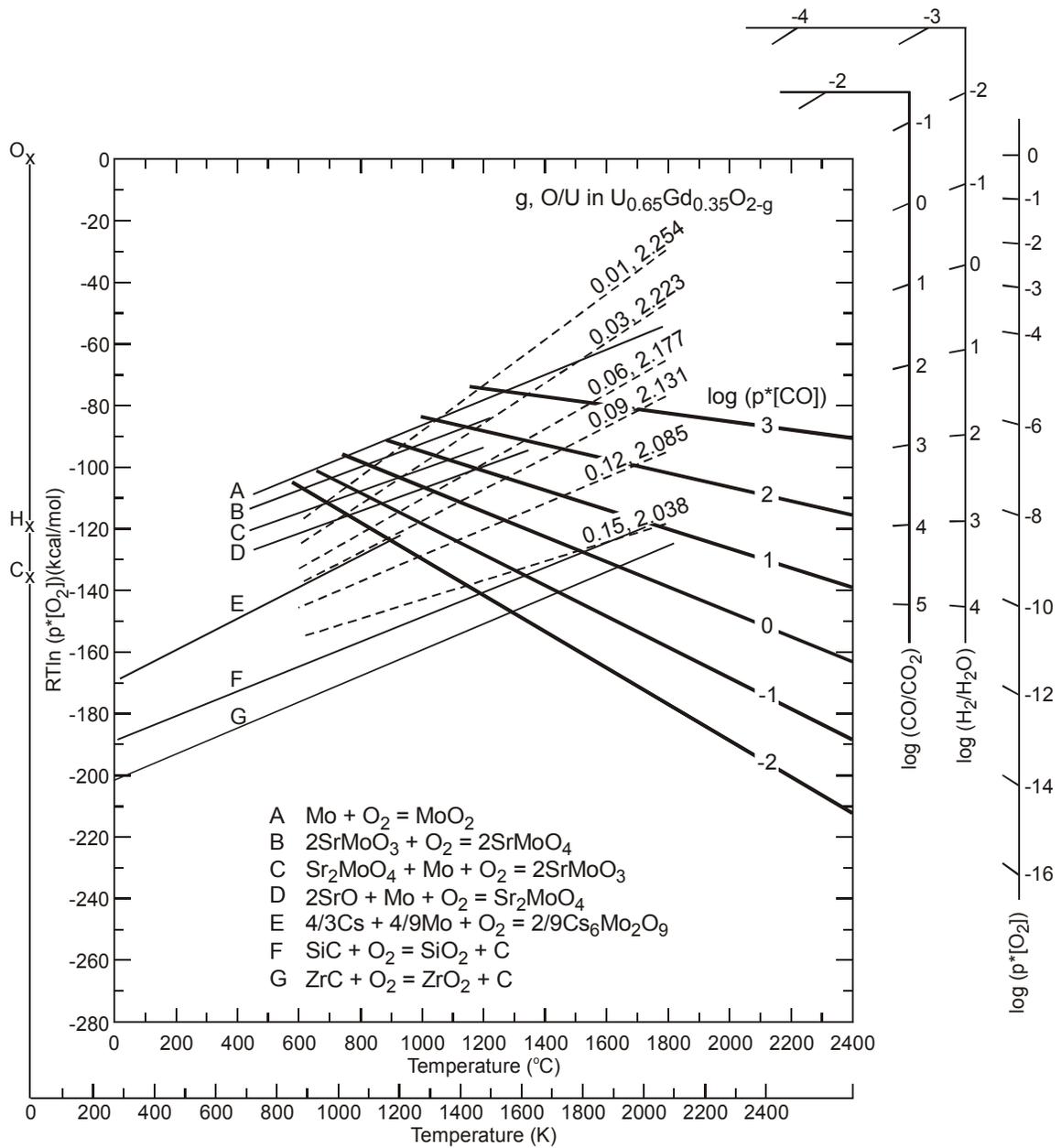
Fig. 4. The Ellingham diagram for several equilibria relevant to the chemistry of fuel performance. (The characteristics of $U_{0.65}Gd_{0.35}O_{2-g}$ are illustrated.)

19
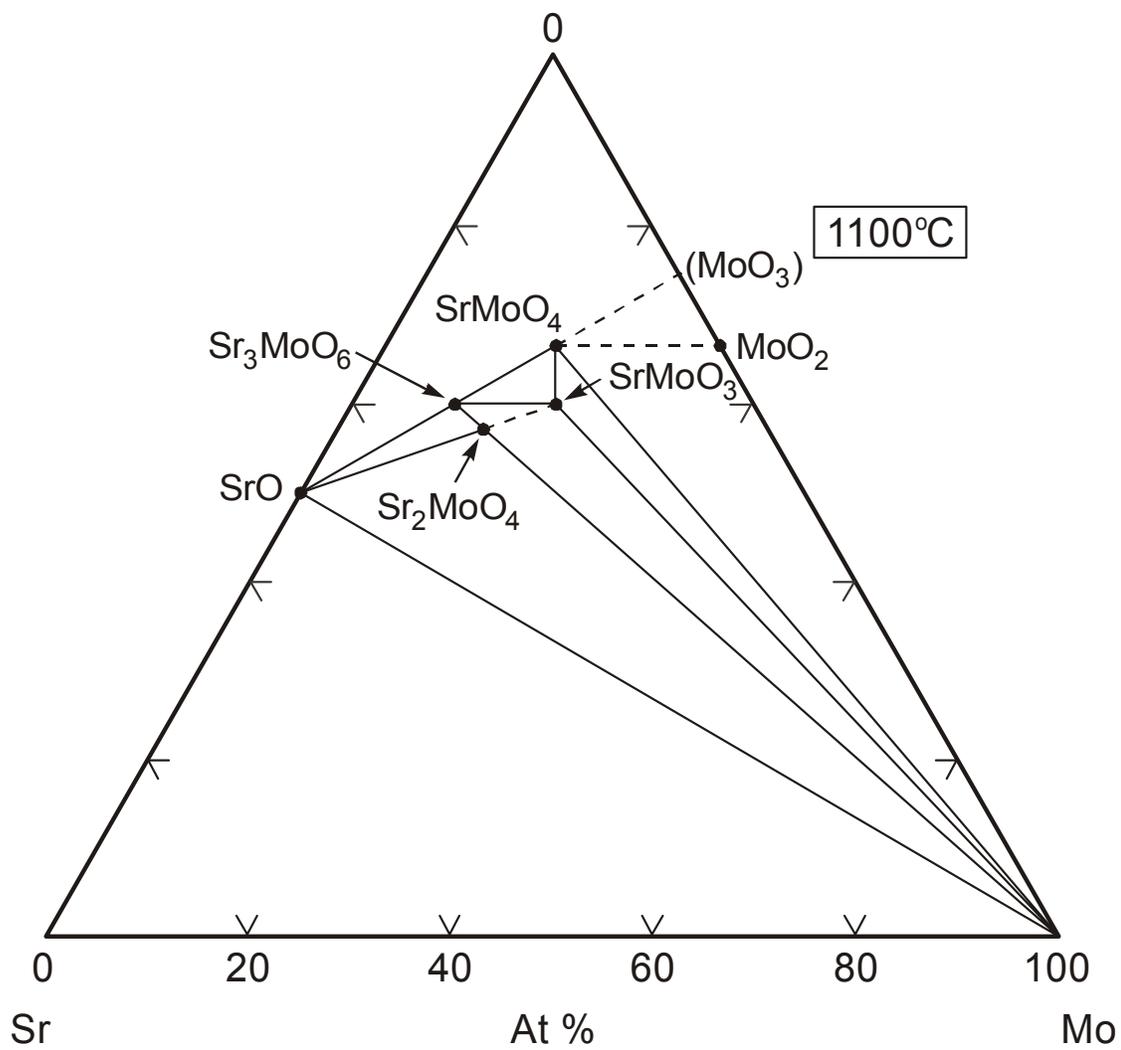
Fig. 5. The Sr-Mo-O ternary phase diagram at 1100 °C.
(Solid MoO_3 does not exist at this temperature.)

Lindblom and Rosen's determination of $p^*[O_2]$ for the equilibrium $Mo + 2 SrO + O_2 = Sr_2MoO_4$ from 1209 to 1565 K resulted in $\log(p^*[O_2]) = -13.471 - 31,012/T + 2.619 T\ln(T)$. This equation was evaluated here at 1200 and 1600 K and led to the corresponding oxygen potential that was represented by $RT\ln(p^*[O_2])$ (cal/mol) $= -158,160 + 37.1T$. This is plotted in Fig. 4. As Lindblom and Rosen note, the value of ΔG^o_f (Sr_2MoO_4) is obtained by adding to this $2\Delta G^o_f$ (SrO) (cal/mol) $= 2(-142,436 + 24.813T)$, as determined here from the 1200 and 1600 K data from Pankratz (ref. pa82), and one obtains ΔG^o_f (Sr_2MoO_4) (cal/mol) $= -443,032 + 86.726 T$. Their 1202–1349 K study of the equilibrium $SrMoO_3 + 0.5 O_2 = SrMoO_4$, an equilibrium that is also in equilibrium with Mo, Fig. 5, resulted in $\log(p^*[O_2]) = -6.5553 - 28,178/T + 1.7737\ln(T)$ for the equilibrium involving $0.5 O_2$. The corresponding oxygen potential was obtained by multiplying their 1300 and 1473 K data, their Table 5, by $2/(8.314/1.987)$ and fitting it to give $RT\ln(p^*[O_2])$ (cal/mol) $= -140,158 + 36.829T$, which is also plotted in Fig. 4. Their phase diagram also indicates that $SrMoO_4$ is in equilibrium with MoO_2; note that MoO_3 melts at 1075 K. They did not study the equilibrium $Sr_2MoO_4 + Mo + O_2 = 2 SrMoO_3$, but the oxygen potential by definition lies between the two equilibria labeled B and D in Fig. 4 and is derived next. First, ΔG^o_f ($SrMoO_4$) can be derived from ref. ku79, which lists $\Delta H^o_{f,298}$ (Sr_2MoO_4) $= -50,700$ cal/mol from the component oxides. This value, plus $\Delta H^o_{f,298}$ for SrO and MoO_3 and the 1200 and 1500K free energy functions for Sr, O_2, Mo, SrO (from ref. pa82) and MoO_3 (from ref. st71) were used to calculate ΔG^o_f ($SrMoO_4$) at 1200 and 1500K; it is assumed here that the free energy function for $SrMoO_4$ equals the sum of the component oxides. A fit of this data led to ΔG^o_f ($SrMoO_4$) (cal/mol) $= -363,750 + 77.93T$. Then, this was used with Lindblom and Rosen's $RT\ln(p^*[O_2])$ (cal/mol) $= -140,158 + 36.829T$ for the equilibrium $2 SrMoO_3 + O_2 = 2 SrMoO_4$ to obtain ΔG^o_f (Sr_2MoO_4) (cal/mol) $= -293,671 + 59.51T$. Thus all needed thermodynamic data is available to calculate the oxygen potential for the equilibrium $Sr_2MoO_4 + O_2 = 2 SrMoO_3$, which leads to $RT\ln(p^*[O_2])$ (cal/mol) $= -143,910 + 32.29T$, which is also plotted in Fig. 4 as equilibrium C.

There are thermodynamic effects in the $Sr-Mo-O_2$ system that were not included in the calculations to be developed below. It was simply assumed that Mo, Sr_2MoO_4, and SrO were present at unit activity. As can be seen from Fig. 4, this phase affects the lower-temperature data; it is not stable at the higher temperatures at the oxygen potentials of the fuel. Other effects can be deduced from the equilibrium constant for $Mo + 2 SrO + O_2 = Sr_2MoO_4$, which leads to $RT\ln(p^*[O_2]) = -RT(\ln[a_{Mo}] + 2\ln[a_{SrO}]) + \Delta G^o_{rx}$, in which a_{Mo} and a_{SrO} are the chemical activities of Mo and SrO, respectively. Solution of Mo in an intermetallic phase, or its presence as a carbide, or solution of SrO in the actinide oxide all reduce their chemical activity below unity and may increase the oxygen potential for the equilibrium beyond that for the fuel. (Or, equivalently, shift the equilibria shown in Fig. 4 at a given oxygen potential to lower temperatures.) For example, $\Delta H^o_{f,298}$ (kcal/mol) $= -11.0$ for Mo_2C (Table A, ref. ku79) and its presence would make the oxygen potential of the above equilibrium more positive by 5.5 kcal/mol. SrO is slightly soluble in UO_2 and even if it were present as an ideal solution it would have a similar effect. For the case of analogous phase behavior in the Ba-Mo-O system, the combined effect of Ba + Sr from Table 1 on the O/f is seen to decrease for fission in heavier actinides (50% from [233]U fission to [241]Am fission).

7.3 REVIEW OF O/f MEASUREMENTS IN $Th_{1-w}U_wO_2$ FUEL PARTICLES

There are two publications containing O/f measurements in irradiated $Th_{1-w}U_wO_2$ fuel particles (refs. li77, pr85). Proksch, Strigl and Nabielek (PSN) (ref. pr85) investigated particles for which Th/[235]U ranged from 4.3 to 48.5 (a range of w from 0.19 to 0.02), with 70% of the particles having w values of 0.14 to 0.19. Burnup ranged from 4.1 to 16.8% FIMA and particles were broken after heating at 800 to 2000°C. They represented their data by

$$\log (O/f) = 0.96 - 4,420/T + 0.4\log([1-w]/w) + 0.3\log(f). \qquad (7.3)$$

21

and at w = 0.18 this reduces to

$$\log (O/f) = 1.61 - 4,420/T + 0.3\log(f) \qquad (7.4)$$

The present author (ref. li77) studied BISO-coated ThO_2 particles that were irradiated up to 17.7% FIMA of the bred-in uranium to give w ranging from about 0.03 to 0.1 with 75% ^{233}U fission and 25% ^{235}U fission, plus one set of $Th_{0.81}U_{0.19}O_2$ particles irradiated up to 23.1% FIMA, with about 33% ^{233}U fission and 67% ^{235}U fission. Particles were heated from 1050 to 2000°C and broken to measure the CO and Kr + Xe release. Measurements for three particles from Proksch and Strigl gave O/f results identical to theirs. The ORNL results were represented by

$$O/f = 74.6f \exp(- 7,400/T) \qquad (7.5)$$

and is rearranged for comparison with the PSN equation to give

$$\log(O/f) = 1.87 - 3,213/T + \log(f). \qquad (7.6)$$

The data in ref. li77 were reexamined thoroughly and led to a better fit of the data. A least-squares fit of the data confirmed the O/f equation given above, with the coefficient on log(f) being close to unity and not the 0.3 of the PSN equation. However, the above equation predicted O/f values considerably higher than the experimental data at 23% FIMA, and a different representation was sought. A plot of the original oxygen potential data revealed that, given the scatter in the data, the oxygen potential was constant with temperature at a given burnup over the entire 900 K range. A least-squares fit of the oxygen potential data also revealed no significant dependence on temperature. Also, the oxygen potential at a given temperature was reasonably linear with ln(f), and later thermodynamic calculations at 1400 K revealed the same dependence. Thus a least-squares fit of the entire oxygen potential data base in ref. li77 was performed. A correction was made to the typographical error in the last data point for HT-13-8/2 to give -102 kcal/mol, and the data sets having O/f values of 0.355, 0.376, 0.452 and 0.492 were excluded. The fit led to

$$RT\ln(p^*[O_2]) \text{ (cal/mol)} = - 75,789 + 8,011 \ln(f). \qquad (7.7)$$

The corresponding O/f equation can be calculated from the relationships for CO in Sect. 3, namely, $RT\ln(p^*[O_2])$ (cal/mol) $= 2 RT\ln(p^*[CO]) - 54,190 - 41.528 T$. The fuel particle can be considered to contain one mole of actinide oxide, a free volume in the buffer of v' times the molar volume of the kernel, V_m, and an ideal-gas law pressure, $p^*[CO] = n_{CO}R'T/(v'V_m)$. Here n_{CO} is the moles of CO (as used here, the "O" in O/f), R' = 82.06 cm^3 atm mol^{-1} K^{-1} and in the thoria particles $v'V_m = 0.5(26.4)$. Upon equating the two oxygen potential expressions one obtains

$$- 75,789 + 8,011 \ln(f) = 2 RT\ln(82.06n_{CO}T/13.2) - 54,190 - 41.528 T \qquad (7.8)$$

and rearrangement of the terms leads to

$$\ln(n_{CO}) = \ln(O) = (- 5,027 + 2,016\ln(f))/T + 8.351 - \ln(T). \qquad (7.9)$$

Subtracting ln(f) from both sides leads to

$$\ln(O/f) = - 5,027/T + \ln(f)(2,016/T - 1) + 8.351 - \ln(T). \qquad (7.10)$$

22

This equation led to the sum of the square of the residuals in ln(O/f) that were 41% of those from the original equation of ref. li77, that represented the 23% FIMA oxygen potentials much better, and that gave values of O/f at 23% FIMA that, unlike the original equation, did not exceed the theoretical limit of 0.36.

Thermodynamic calculation of O/f values permitted a check of the sensitivity of O/f on the buffer layer volume in the six different particle types in ref. li77. The thermodynamic calculations of O/f used the above CeO_{2-c} and $U_{1-z}Gd_zO_{2-g}$ solid solution models that were not available when the O/f data were developed. Each measurement in ref. li77 was tabulated along with kernel radius and buffer-layer thickness, which permitted calculation of the void volume available for gases upon assuming that the buffer layer was 50% of theoretical density. The void volume ranged from 0.21 to 0.62 of that in the kernel in particles that initially contained ThO_2 kernels to 1.44 in $Th_{0.81}U_{0.19}O_2$ fuel particles, the latter achieving about 23% FIMA. A standard particle containing a relative void volume of 0.5 was assumed and calculations for the thoria particles were performed at 5% FIMA at 1800 K; the O/f relative to the standard particle ranged from 0.84 to 1.03. The relative O/f in the thoria-urania particle was calculated at 23% FIMA and was 1.16 of that in the standard particle at 23% FIMA. It was concluded that the variations in the void volume had little effect on the experimental O/f values that are represented by the equations above, especially when one considers the scatter in the original measurements.

At this juncture the results of the two experimental sets of measurements represented by the equations above are compared. The results are given below, with the first value of O/f calculated from the PSN equation and the second calculated from the new Lindemer (TBL) equation, both for TBL conditions.

Table 2. Comparison of PSN[a] and Lindemer[b] O/f values in $Th_{1-w}U_wO_2$ fuel particles

| FIMA | w | Temperature (K) | | | | | |
| | | 1400 | | 1800 | | 2200 | |
		PSN	TBL	PSN	TBL	PSN	TBL
0.05	0.07	0.0071	0.022	0.034	0.101	0.094	0.252
0.15	0.09	0.0089	0.0082	0.047	0.115	0.125	0.230
0.23	0.10	0.0097	0.044	0.048	0.121	0.136	0.222

[a] From Eq. 7.3.
[b] From Eq. 7.10.

It is clear that the PSN equation gives O/f values considerably lower than those from the new Lindemer equation (as well as those from the original equation), but the reason for this difference is unknown, particularly in view of the fact that identical particles studied by both sets of authors gave the same O/f values.

7.4 O/f CALCULATED FOR $Th_{1-w}U_wO_2$ FROM THERMODYNAMIC MODELING

The thermodynamics of the ceria, urania-gadolinia and Sr_2MoO_4-Mo-O_2 systems, along with those for CO and CO_2, were used to calculate O/f values for the conditions of ref. li77. The uranium content of 0.07 to 0.08 per initial mole of thorium was obtained from Fig. 2 of ref. li77 and included the uranium derived from decay of ^{233}Pa in that set of particles. This became the uranium content in $U_{1-z}Gd_zO_{2-g}$. The moles of Y and three-valent lanthanides were calculated from the yields in Sect. 7.1 as 0.41 f for the case of ^{233}U fission. Thus z = 0.41 f/(0.41 f + 0.07 to 0.08); we will continue to use Gd in the text, but it represents these fission products. Several assumptions were made in order to perform these calculations. It was assumed that the free volume in the buffer layer was 0.5 of the kernel volume. The effect of the solution of ceria in $U_{1-z}Gd_zO_{2-g}$ is an unknown and two assumptions were made, one set with ceria in the solution, in which case z = 0.54 f/(0.54 f + 0.07 to 0.08), and one without. In addition, CeO_{2-c} was always included as a separate phase in the O/f calculations. Inclusion of the Sr_2MoO_4-Mo-O_2 system presented two more assumptions, the first being that the thermodynamic behavior of the Ba-Mo-O_2 system was identical to that for the Sr-Mo-O_2 system and the second that only BaO was present. All phases are

assumed to be present at unit activity. The calculations were performed in a spreadsheet by an iterative technique. At a given temperature and burnup the initial amount of CO was calculated from the author's new equation. This was used to calculate p*[CO] using the ideal-gas law (see the previous section) and thus the oxygen potential was calculated. The values of g in $U_{1-z}Gd_zO_{2-g}$ and c in CeO_{2-c} were then determined by manual iteration until they gave the same oxygen potential. An oxygen balance was then determined, as follows. The maximum moles of released atomic oxygen were 0.36 f, from Sect. 7.1 for [233]U. From this was subtracted the moles of atomic oxygen combined in CO, CO_2, $U_{1-z}Gd_zO_{2-g}$ (beyond that in UO_2 and $GdO_{1.5}$), CeO_{2-c} (beyond that in $CeO_{1.5}$) and in the MoO_2 in Sr_2MoO_4. Initially this resulted in positive or negative moles of oxygen atoms unaccounted for, and thus the initial amount of CO was adjusted to accommodate this oxygen imbalance, which gave a new oxygen potential for which new values of g and c were calculated. After a few iterations the final oxygen balance was zero and the O/f was calculated from the moles of CO and CO_2 and the burnup.

The sensitivity of the different assumptions concerning ceria and baria on the calculations was assessed at several temperatures and burnups and typical results are shown in Table 3. It can be seen that the range of oxygen potential is about 10 kcal/mol and that the O/f varies by about a factor of 7. The author's experimental results would lead to one set of thermodynamic assumptions and the PSN experimental results would lead to an entirely different set. One might conclude that the ranges shown in Table 3 represent the uncertainty in both the thermodynamic and experimental approaches to measuring O/f.

Table 3. Effect of assumptions on the thermodynamic calculations at 1400 K and 5% FIMA

Assumption	Oxygen potential (cal/mol)	O/f
Sr_2MoO_4, no ceria in $U_{1-z}Gd_zO_{2-g}$	-98,940	0.026
Sr_2MoO_4, ceria in $U_{1-z}Gd_zO_{2-g}$	-104,000	0.104
$(Sr,Ba)_2MoO_4$, no ceria in $U_{1-z}Gd_zO_{2-g}$	-106,700[a]	0.0065
$(Sr,Ba)_2MoO_4$, ceria in $U_{1-z}Gd_zO_{2-g}$	-106,700[a]	0.0065
new Lindemer data fit	-99,800	0.022
PSN equation	-106,100	0.0071

[a] This system was at the $(Sr,Ba)_2MoO_4$-Mo-O_2 equilibrium with part of the Mo as $(Sr,Ba)_2MoO_4$

Since the assumption of Sr_2MoO_4 and no ceria in $U_{1-z}Gd_zO_{2-g}$ led to agreement with the author's new fit of his data, this set of conditions was used here for the more extensive calculations given in Table 4.

Table 4. Comparison of calculated and experimental O/f and oxygen potential values (kcal/mol) for $Th_{1-w}U_wO_2$

FIMA	Temperature (K)							
	1250		1400		1600		1800	
	O/f	kcal/mol	O/f	kcal/mol	O/f	kcal/mol	O/f	kcal/mol
0.05 calc'd	0.0070	- 101.4	0.026	- 98.9	0.064	- 98.5	0.220	- 94.2
data	0.0097	- 99.8	0.022	- 99.8	0.052	- 99.8	0.101	- 99.8
0.15 calc'd	0.014	- 93.6	0.040	- 91.2	0.080	- 90.5	0.120	- 90.9
data	0.019	- 91.0	0.036	- 91.0	0.070	- 91.0	0.115	- 91.0

Several observations can be made from these results. The increase in O/f with temperature is the result of more reducing conditions as temperature is increased, with the result that there is more oxygen in CO and correspondingly less in the urania-gadolinia and ceria. The results from the thermodynamic approach are in very close agreement with the experimental data, but it can be seen that there is a slight

temperature trend in the thermodynamic calculations that is not represented in the new fit of the data. The thermodynamic approach is probably acceptable for calculating p*[CO], especially for pressure-vessel mechanical considerations. The thermodynamic approach has the possible advantage of calculating O/f values under conditions beyond the experimental conditions that led to the PSN and Lindemer O/f equations.

7.5 O/f CALCULATED FOR UO_2 FROM THE THERMODYNAMIC MODEL

Proksch, Strigl, and Nabielek (PSN) (ref. pr82) published measurements of O/f in UO_2 kernels enriched in [235]U from 0.7 to 93% and irradiated from 0.7 to 70% FIMA. PSN report fission contributions from [235]U, [239]Pu, and [241]Pu but give no data on the relative contributions to total burnup; they concluded that their data revealed no dependence of O/f on the actinide that fissioned. Their results were not only dependent on burnup and temperature, but on time in reactor and were represented by

$$\log(O/f) = -0.21 - 8,500/T(K) + 2\log(t) \tag{7.11}$$

in which t is in-reactor time in days. As PSN note, the time dependence of this equation restricts its use to the irradiation conditions for the original particles. Application of their equation at 200 days and 1400, 1600, and 1800 K, values that are within their experimental values, give O/f values of 0.021, 0.139, and 0.532, respectively, with the latter being beyond that possible for their conditions and beyond their maximum measured value. Such calculated results probably prevent the application of the PSN equation to fuels irradiated for much longer times in a power reactor since the equation generally gives impossible O/f values at these longer times.

Given the difficulty of using the above equation, the thermodynamic approach was applied to fission of $^{235}UO_2$. The approach used in the previous section was used at an assumed gas volume in the buffer layer of 3.5 times that in the kernel. The atmosphere contained substantial CO_2 at 1400 K and thus the O/f calculation included contributions from both CO_2 and CO. The results are given in Table 5.

Table 5. O/f and oxygen potential (kcal/mol) calculated from the thermodynamic model for $^{235}UO_2$

FIMA	Temperature (K)					
	1400		1800		2200	
	O/f	kcal/mol	O/f	kcal/mol	O/f	kcal/mol
0.10	0.106	-97.7	0.190	-103.6	0.309	-108.0
0.25	0.113	-92.4	0.204	-96.6	0.300	-100.5
0.50	0.139	-87.6	0.246	-90.2	0.326	-93.7
0.75	0.246	-82.8	0.297	-86.0	0.356	-89.3

These calculated results are relatively independent of burnup until high burnup and is a result of the rapid change in z in $U_{1-z}Gd_zO_{2-g}$ at high burnup.

7.6 EFFECT OF OTHER OXIDE FORMERS

Inclusion of the other oxide formers could reduce the calculated O/f values given above for urania. For example, Kleykamp, in his extensive analysis of chemical behavior in irradiated oxide fuels (ref. kl85), includes an analysis of the solubility of Ba, Sr, and Mo in the oxide phases in light-water and fast-breeder reactor fuels. He observes that lower temperatures and higher oxygen potentials lead to increased solubility of these elements in the actinide oxide. The solubility of molybdenum may be 5% per his Fig. 23 at O/Mo = 2 and this would clearly lower the O/f values in the above tables, at least at lower temperatures. Such solubility would effectively lower the Mo-MoO_2 equilibrium shown in Fig. 4 by

RTln(activity of MoO_2) as long as elemental Mo was also present. Phase diagrams also indicate similar low solubilities of SrO. The solution effect of SrO could promote the O/U value because of the resulting oxygen vacancies in the urania lattice—this would also lower the O/f values.

The possibility of metal-oxide equilibria in the Cs-Mo-O system that affects the oxygen potential in the fuel particles is considered next. Kleykamp reports measurement of Cs solubility up to 0.012 mole fraction, presumably as "CsO_2" (ref. kl85). There are Cs-Mo-O phases in the system as shown in Fig. 6, but the highest known melting temperature is 1215 K, for Cs_2MoO_4, which is in equilibrium with Mo and MoO_2 (ref. jo81) at the oxygen potentials shown in Fig. 4. The phase diagram at the fission-product Cs/Mo value of ~ 0.66 or Cs_2O/MoO_3 of ~ 0.33 indicates that liquids would be present as low as 460°C (ref. ro95). The $Cs_6Mo_2O_9$-Cs-Mo equilibrium probably lies at the most negative oxygen potential (ref. jo81) and is shown in Fig. 2 up to 1215 K even though Cs-Mo-O liquids would undoubtedly be present also. If the $Cs_6Mo_2O_9$ were present in the fuel particle, it could potentially combine with 1.5 oxygen atoms per Cs and thus combine 0.13(1.5) or ~ 0.2 oxygen atoms. As can be seen by comparing the oxygen potential in Fig. 4 for this phase with Fig. 2, however, this would not appear to substantially reduce the oxygen potential of the Pu-O fuel system since the $Cs_6Mo_2O_9$-Cs-Mo equilibrium lies above that for O/Pu ~ 2 for T < 1215 K.

7.7 OXYGEN RELEASE FOR PuO_{2-x}

Consider next the effect of oxygen release in a driver or transmutation fuel containing a PuO_{2-x} kernel. Here the oxygen released by fission, 0.87-x, has no alternative but to increase the oxygen potential as both an increase in CO pressure and the O/Pu of the remaining fuel. No oxide equilibria other than those in the Pu-C-O-stable oxide system are being considered because there is no basis in the literature for O/Pu > 2 or O/(Y, Lanthanide) > 1.5 in the Pu-O-lanthanide phases. The in-particle CO pressure is calculated from the ideal-gas law by conveniently assuming a kernel containing one mole or ~ 23 cm^3 of plutonia. The present DF and TF fuels have a free volume in the buffer of 3.5 times the kernel volume, and thus, since R/ v'V_m = 82.06/(23 x 3.5) $\cong$ 1, one obtains

$$p(CO) \text{ (atm)} = nT. \tag{7.12}$$

Here n in general is the total moles of all gases (CO, Kr, Xe, He, Cs, Rb), but for the present purposes is the moles of CO and CO_2 that is not combined in the stable oxides and the remaining plutonia. For example, if the transmutation fuel were 100% $AmO_{1.5}$ and 75% of it were fissioned, at 1500 K, p(CO) = 0.75(0.46)1500 = 517 atm. The effect of the oxygen release can be seen qualitatively in Fig. 2, where the interdependence of p(CO), O/Pu and T are plotted. Here it can be seen that at T < ~ 1100°C, oxygen release by fission to form CO is negligible at p(CO) < 10 atm (n < 0.007) and the O/Pu can reach nearly 2. If f_2 is defined as the fraction FIMA at which O/Pu = 2, the value of f_2 is obtained from the oxygen balance,

initial oxygen = oxygen in fission products + oxygen in remaining PuO_2

$$2-x = 1.13 f_2 + 2 (1- f_2) \tag{7.13}$$

which is rearranged to obtain

$$f_2 = x/0.87. \tag{7.14}$$

Thus, for initial O/Pu values of 1.8, 1.7, 1.6 and 1.5 (x = 0.2, etc.) the O/Pu of the remaining fuel approaches 2 at 23.0, 34.5, 46.0 and 57.5 % FIMA, respectively. For f > f_2, the oxygen released as CO, n_{CO}, from the remaining PuO_2 is then

$$n_{CO} = (2-1.13)(f - f_2) = 0.87 (f - x/0.87) = 0.87f - x , f > f_2. \tag{7.15}$$
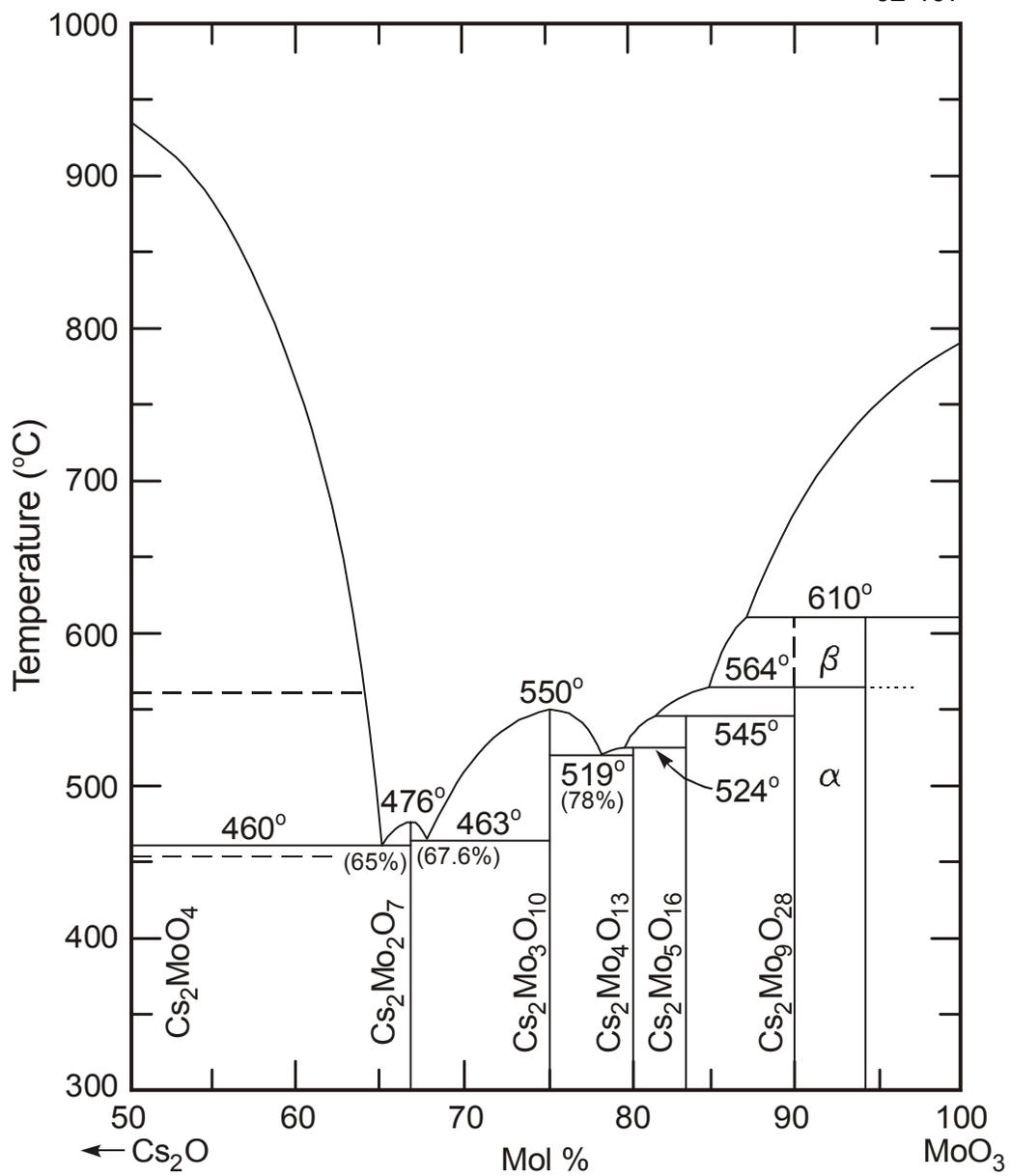
Fig. 6. The partial phase diagram for the Cs₂O-MoO₃ system.

The Pu-Am transmutation fuel can be treated similarly by taking a weighted average of the oxygen combined in the strong oxide formers, a value of 2 - x = O/(Pu + Am), and f from the combined fission of both actinides.

A more quantitative approach was performed for the plutonia system by spreadsheet calculations similar to those used previously for the thoria-urania systems. The calculations assumed equilibrium in the Pu-O and Ce-O systems at unit activity of each at an oxygen potential established by the C-CO equilibrium. The spreadsheet calculations were again iterated manually until the oxygen released by fission was accommodated in the CO, CO_2, CeO_{2-c} and the remaining PuO_{2-x}, which had an O/Pu different from the initial value, again with the C-CO, C-CO_2, ceria, and plutonia systems at the same oxygen potential. The free volume in the buffer layer was 3.5 times that in the kernel. Tabulation of O/f in this context was deemed meaningless; instead, the p*[CO] + p*[CO_2] (in units of atmospheres) and final O/Pu is given in the following table. These calculations indicate that substantial CO and CO_2 pressures will be achieved at high burnup even at an initial O/Pu = 1.6, which is probably the lowest that can be achieved practically by hydrogen reduction. The approximate oxygen potential for the results in Table 6 can be found by interpolating the CO pressures onto Fig. 2, while a more exact calculation can be obtained from the PuO_{2-x} model.

Table 6. Gas pressure (CO + CO_2) and O/Pu values calculated for fission of PuO_{2-x}

Initial O/Pu	FIMA	Temperature (K)					
		1400		1800		2200	
		Pressure (atm)	O/Pu	Pressure (atm)	O/Pu	Pressure (atm)	O/Pu
1.9	0.10	6.4	1.978	155	1.888	394	1.786
1.9	0.25	152	1.997	321	1.911	586	1.799
1.9	0.50	439	1.998	646	1.931	934	1.814
1.9	0.75	729	1.999	985	1.941	1300	1.824
1.8	0.10	0.2	1.873	46	1.845	223	1.762
1.8	0.25	24	1.990	172	1.891	389	1.786
1.8	0.50	304	1.998	475	1.922	726	1.805
1.8	0.75	590	1.999	811	1.936	1087	1.818
1.7	0.10	0.01	1.76	4.4	1.761	63	1.731
1.7	0.25	0.21	1.886	51	1.850	206	1.766
1.7	0.50	169	1.997	310	1.910	522	1.795
1.7	0.75	454	1.998	637	1.930	875	1.811
1.6	0.10	0.001	1.652	1.7	1.652	3.4	1.652
1.6	0.25	0.011	1.755	3.5	1.754	54	1.726
1.6	0.50	33	1.9922	154	1.888	322	1.780
1.6	0.75	314	1.9986	466	1.922	663	1.802

7.8 MITIGATION OF OXYGEN RELEASE BY THE UC$_2$-UO$_2$ KERNEL OR ZrC

The oxygen released during fission can be accommodated by an oxide-carbide fuel kernel in the uranium and plutonium systems. In the UC$_2$-UO$_2$ fuel kernel, the so-called U(C,O) or oxycarbide fuel, the fuel and fission-product carbides reacted with the released oxygen to form the highly stable oxides and thus kept the CO pressures negligible and the oxygen potential low enough to prevent kernel migration (ref. ho77). This same technique could be applied to the driver fuel with a $PuO_{1.5}$-$PuC_{1.5}$ kernel, where

the oxygen release, 0.87 - 0.5 = 0.37, would be very similar to the 0.41 for uranium fission and thus the required carbide content described in ref. ho77 could be used. Unfortunately, this technique cannot be used for the transmutation fuel, as discussed in the section above concerning the thermodynamics of americium carbide.

Another means to getter the oxygen release is incorporation of ZrC in the particle (refs. bu83, bu84). This has been studied with the ZrC dispersed in the buffer-layer pyrocarbon or as a solid layer over a kernel having a seal coat of pyrocarbon. The relevant equilibrium for reaction of oxygen with ZrC is

$$ZrC + O_2 = ZrO_2 + C \tag{7.16}$$

for which, with JANAF data (ref. st71), the oxygen potential is

$$RTln(p*[O_2]) \text{ (cal/mol)} = - 213,840 + 41.75T. \tag{7.17}$$

This is plotted on Fig. 4. The moles of ZrC needed to getter the oxygen released by fission of americium, 0.46/f , Table 1, would be 0.23 times the expected americium burnup. At 75% FIMA this would amount to 0.17 moles of ZrC per mole of kernel. The ZrC requirement for the plutonia component of the driver and transmutation fuels would be greater. The ZrC would getter any oxygen beyond O/Pu = 1.5 in the PuO_{2-x}. The reduction to O/Pu = 1.5 should occur in the early part of the irradiation and would consume (2-x - 1.5)/2 or (0.5 - x)/2 moles of the ZrC per mole of plutonia in the kernel, while oxygen released during fission would require an additional 0.38/2 moles of ZrC per mole of plutonia that fissioned. These requirements lead to a ZrC coating thickness that is roughly 5–10% of the kernel radius. To these requirements would be added the need for maintaining an intact ZrC coating.

Factors affecting the performance of the ZrC would have to be established. Gettering of the oxygen would require that the inner seal coat be breached early in the irradiation. Whether the CO-ZrC reaction rate at normal fuel temperatures to form zirconia and carbon via the reaction $ZrC + CO = ZrO_2 + 3\ C$ would be fast enough to getter the oxygen would need to be established. Given that the molar volumes of ZrC, zirconia, and carbon are 15.34, 22.0 and 5.33 cc/mol, respectively, 15.34 cc of ZrC reactant is replaced by 22 + 3 x 5.33 or 38 cc of products and this might produce compressive loading of the remaining ZrC layer. The void volume within the initial ZrC layer deposited over a seal coat would seem to be just the few percent of void in a sintered kernel and would lead to extremely high pressures of noble gases. Generation of CO faster than its gettering to form zirconia and carbon would add to these pressures; it seems likely that oxygen diffusion out of the kernel via the crystal lattice would be much faster than diffusion of the noble gases since it is a fact that oxygen diffusion is rapid enough to reduce plutonia in hydrogen in times short compared to in-reactor times. Conversely, reaction of CO as it is generated would reduce the CO pressures to insignificant levels.

8. VAPOR PRESSURE OF CESIUM

Since it appears likely that Cs is in the elemental state in the driver and transmutation fuels, its vapor pressure, which is generally greater than one atm at fuel operating temperatures above 950 K, needs to be represented. The $log(k_{eq}) = log(p*[Cs])$ data from Pankratz (ref. pa82) at 600 and 900 K lead to the equation for p[Cs], the actual pressure of cesium,

$$log(p[Cs], \text{atm}) = - 3,659/T + 3.848. \tag{8.1}$$

This equation provides an upper limit for p[Cs] because the pressure cannot be higher than that over liquid cesium; the triple point of cesium is not considered here. However, at low fuel burnup the pressure may be less than that calculated from the above equation because there is insufficient fission-product cesium available in the gas phase to attain the p[Cs] that is in equilibrium with the liquid. When the

liquid is present, at 951 K p[Cs] = 1 atm, and at the maximum possible fuel temperature of 1600°C, p[Cs] = 78 atm; these pressures are not inconsequential in terms of availability of cesium for diffusive escape from the particle.

9. THE Si-O-C SYSTEM

Thermodynamic values for the Si-O-C system will be calculated because of their relevance to the SiC layer in the coated particle. JANAF data (ref. st71) for SiO gas, SiC and cristobalite at 1000 and 1500 K were used to give

$$\Delta G^o_f\,(SiO_2)\,(cal/mol) = -\ 215,430 + 40.90T \tag{9.1}$$

$$\Delta G^o_f\,(SiO,g)\,(cal/mol) = -\ 25,298 - 19.184T \tag{9.2}$$

$$\Delta G^o_f\,(SiC)\,(cal/mol) = -\ 17,029 + 1.84T. \tag{9.3}$$

The oxygen potential for the equilibrium $SiC + O_2 = SiO_2 + C$ is

$$RTln(p^*[O_2])\,(cal/mol) = -\ 198,392 + 39.06T \tag{9.4}$$

and is plotted on Fig. 4. At this equilibrium the principal gaseous species is SiO and its partial pressure is calculated from the equilibrium

$$0.5\ SiC + 0.5\ SiO_2 = SiO,g + 0.5\ C \tag{9.5}$$

to give

$$p^*[SiO] = exp(-\ [\Delta G^o_f\,(SiO,g) - 0.5\Delta G^o_f\,(SiO_2) - 0.5\Delta G^o_f\,(SiC)]/RT) \tag{9.6}$$

$$log(p^*[SiO]) = -\ 19,875/T + 8.86. \tag{9.7}$$

When the inner pyrocarbon layer in a TRISO particle is cracked during irradiation, attack of the SiC has been observed, e.g., by Minato et. al. (ref. mi91) and Grubmeier et. al. (ref. gr77). At the irradiation temperatures of 1065 to 1685°C reported by Minato et. al. (ref. mi91), the SiO gas pressure from the above equation would be 10^{-6} to 0.051 atm. They provided a thermodynamic analysis that concluded that CO reacted with the SiC to form SiO gas, which transported silicon to the kernel to form the observed (Pd, Ru, Rh, Tc, Mo) silicides.

10. SiC-Pd AND ZrC-Pd REACTION AND THE Ru-Si AND Ru-Zr SYSTEMS

It is well known that Pd, as well as Rh and Ru, react with SiC and ZrC at rates that can be of concern to fuel performance. These elements form intermetallics such as Pd_2Si and $ZrPd_3$ (e.g., refs. mi90, og86, la84, pe80) and the corrosion rates are much higher with SiC than with ZrC (ref. og86). It is of possible concern that at the reaction rate of 10^{-7} microns/sec at even the lowest temperature, 1000°C, reported in Fig. 22 of ref. la84, 10 microns of reaction with the SiC would be attained in 3.2 years. Of further concern is the roughly ten-fold increase in Pd yield from fission of Pu and Am as compared to U fission, plus the additional Pd inventory in the driver and transmutation fuels resulting from higher burnup, all of which may result in a Pd inventory 30–40 times higher than most previous experience. Ruthenium, which is usually associated with Pd in the SiC reaction zone in the laboratory experiments (ref. la84), has a yield higher than Pd, and the two combined add up to about 15% of the total fission products.

30

The qualitative difference in reaction rates between the Si and Zr systems may be explainable in part by the differences in the phase diagrams for Si-C-Pd (refs. wy81, bh96) and Zr-C-Pd (refs. og86, sa71). Consider first the Pd-Si-C system. The compound Pd_2Si exists in equilibrium with C and SiC and the Pd-Si phase diagram of Fig. 7 shows that it melts at 1394°C, which is approximately the temperature where the Pd-SiC corrosion rate reported in ref. la84 begins to increase more rapidly with temperature. The melting temperature is also lower than the maximum possible fuel temperature of 1600°C, and the data indicates that this Pd-Si liquid is a more aggressive corrodant under loss-of-helium-circulation conditions. Below 1394°C the reaction rate changes less rapidly with temperature. As shown in Fig. 7, liquids can still exist in the binary Pd-Si phase diagram between Pd and Pd_2Si as low as 810°C (ref. wy81), and this liquid is present in equilibrium with carbon in the ternary (ref. bh96). The binary between Pd_2Si and Si has liquids in equilibrium with SiC at least as low as 1000°C (ref. bh96). Whether the liquid is present or not depends on rates of mass transport of Pd to the SiC layer by solid-state or gas-phase diffusion from the interior of the kernel and across the pyrocarbon layers as well as the rate of reaction to form the palladium silicides. It is the opinion of the writer that the lower-temperature data for SiC corrosion in Fig. 22 of ref. la84 does not indicate that these low-temperature liquids affect the reaction rate even if they are present; instead, the rate-controlling mechanism would be, e.g., diffusion across the Pd_2Si layer or a solid-state reaction at the Pd_2Si-SiC interface. Ogawa and Ikawa (ref. og86) note that SiC reaction with Pd vapor is much less than that with Pd metal in direct contact with SiC, but the vapor can still result in severe attack. Also, all their reaction rates were considerably higher than those reported in ref. la84. One must also note that even though the fission-product Pd is considerably higher in the Pu- and Am-containing fuels than in the U-containing fuels, the concentration of Pd may or may not affect the reaction rate with SiC. For example, Minato et. al. (ref. mi90) conclude that the reaction rate is controlled by Pd release from the UO_2 kernel, which underwent 4% FIMA; the present particles will undergo much more structural damage during burnup to 75% FIMA and Pd release from the kernel may not be rate controlling here.

Consider next the Pd-Zr-C system. The Pd-ZrC interaction has a reaction rate considerably lower than that for the SiC analog and ZrC-C-$ZrPd_3$ appears to be an equilibrium phase field (ref. og86). The Pd-Zr phase diagram of Fig. 8 (ref. sa71) shows that between Pd and $ZrPd_3$ the lowest melting temperature is that for Pd, 1555°C, while PdZr, $PdZr_2$, and liquids that melt as low as 1030°C appear in the composition range between $ZrPd_3$ and Zr; the $ZrPd_3$ compound melts at 1780 (±25)°C (ref. sa71). The more refractory nature of both ZrC and $ZrPd_3$ when compared with their silicon-containing analogs is postulated to be the reason for the lower Pd-ZrC reaction rate. The fact that there is no liquid phase between solid Pd and $ZrPd_3$ may also be a factor. Finally, post-irradiation examination of both ZrC-TRISO and SiC-TRISO UO_2-fueled particles irradiated to 4% FIMA at 1400 to 1650°C indicated no Pd interaction with the ZrC but severe Pd corrosion of the SiC (ref. mi00); as noted above, only Pd-Si liquids exist in this temperature range.

It is clear that all factors that affect the Pd-SiC reaction rate need to be explored further. It seems that the ZrC-TRISO particle should be considered for the driver and transmutation fuels. Use of either SiC or ZrC as a fission-product barrier should be supported by additional long-time, low-temperature experiments, such as those reported by Lauf et. al. (ref. la84), utilizing both a temperature gradient and isothermal anneals. This should be accompanied by similar post-irradiation examination and anneals in both particle types, and possibly by measurement of consequential release of fission products such as Ag, Cs, Kr, and Xe from the particle.

Consider next Ru, the most abundant noble-metal fission product. The Ru-Si system, Fig 9 (refs. we88, sa78), does not exhibit a liquid on the Ru-rich side of the diagram until 1505°C and the most refractory compound, RuSi, does not melt until 1870°C. Thus Ru would probably be much less likely to corrode SiC at normal reactor operating temperatures. The Ru-Zr system (ref. er88), Fig. 10, also exhibits melting temperatures well above normal reactor operating conditions.
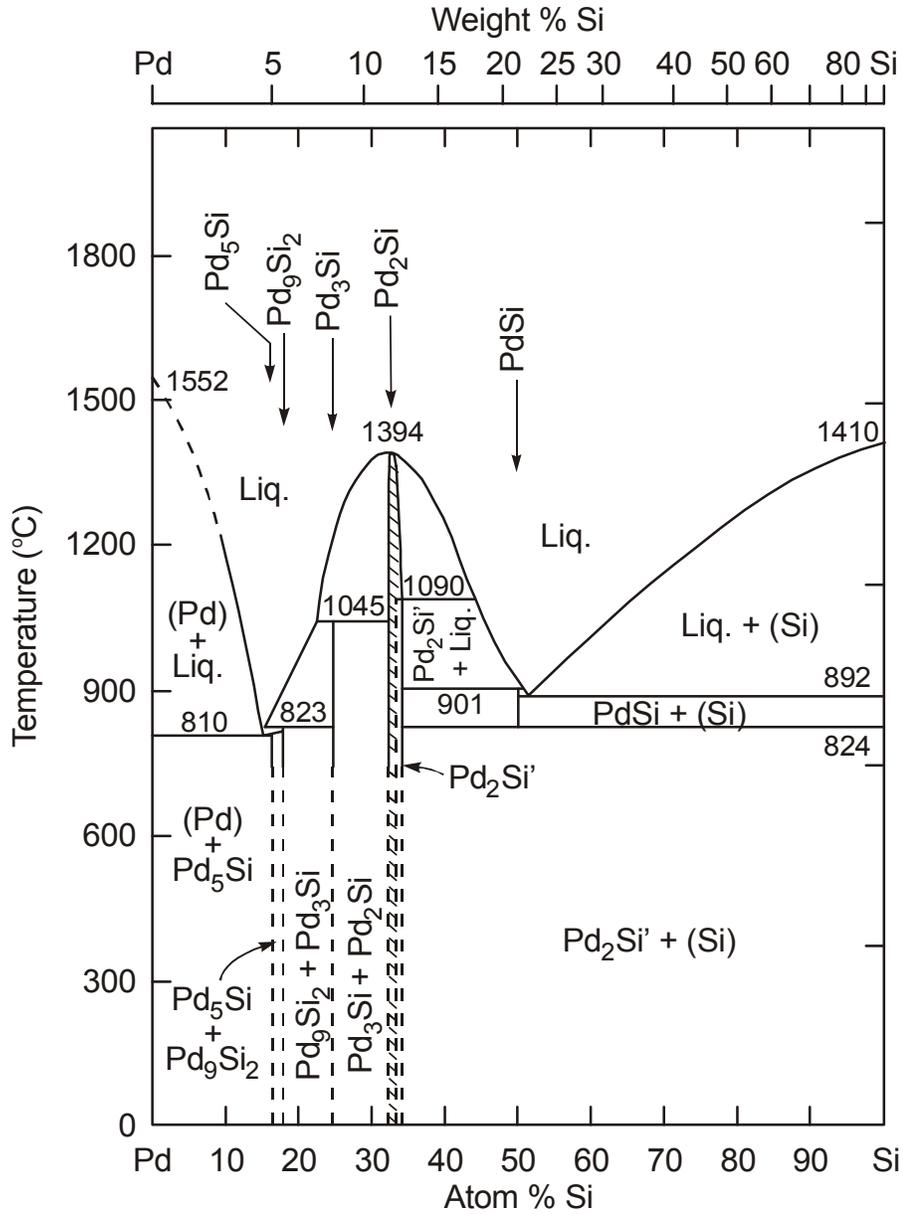
Fig. 7. The Pd-Si phase diagram.
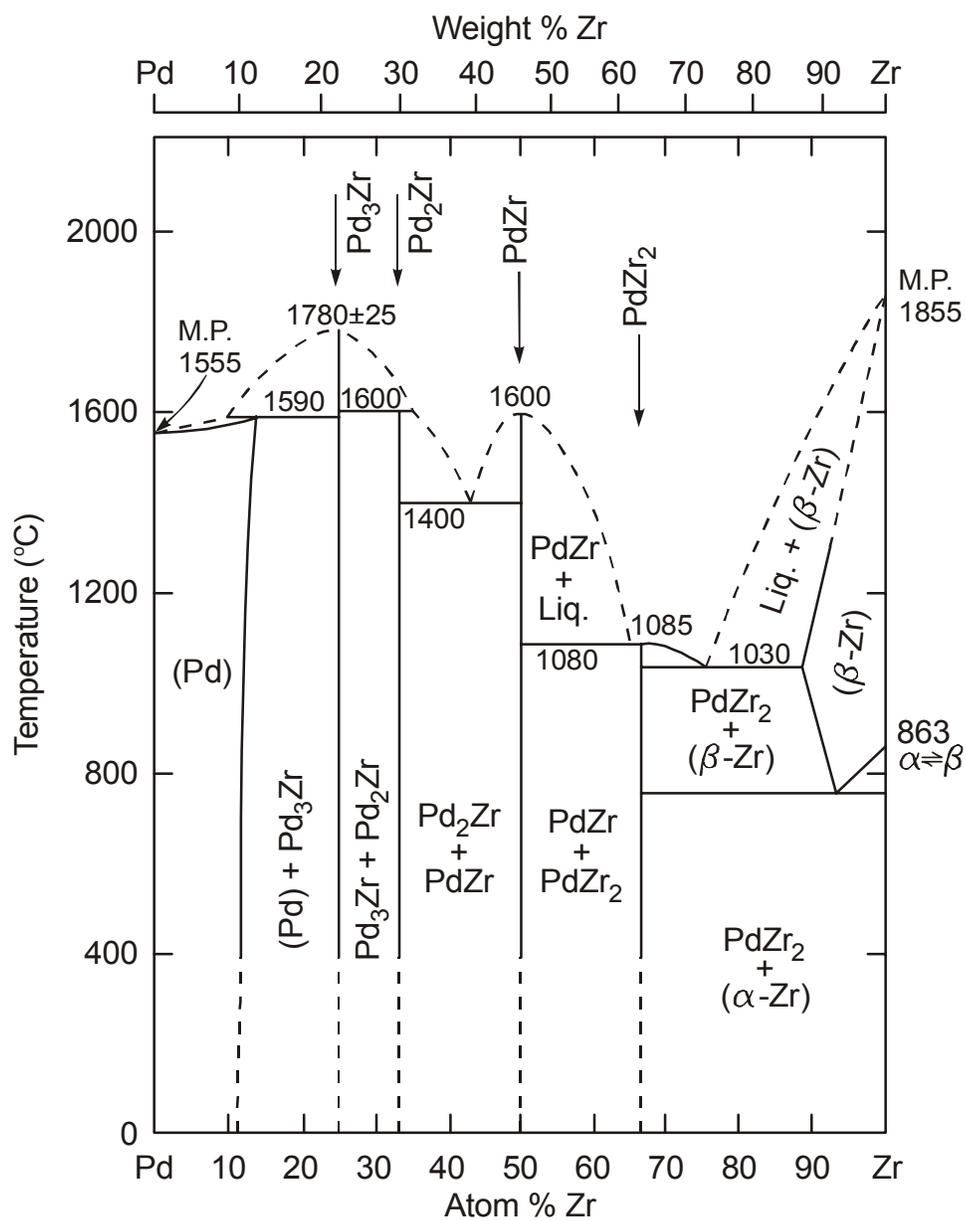
Fig. 8. The Pd-Zr phase diagram.
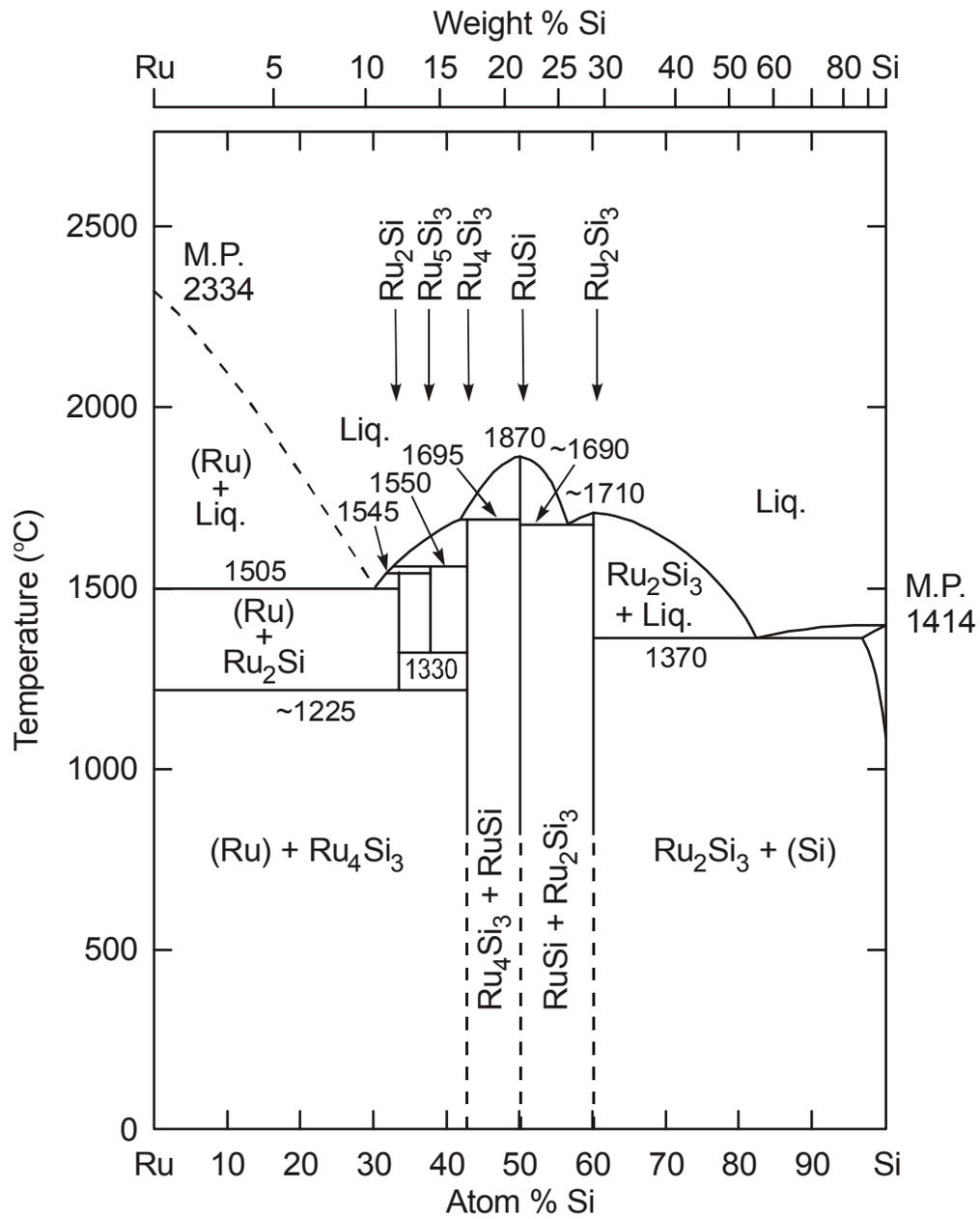
**Fig. 9. The Ru-Si phase diagram.**
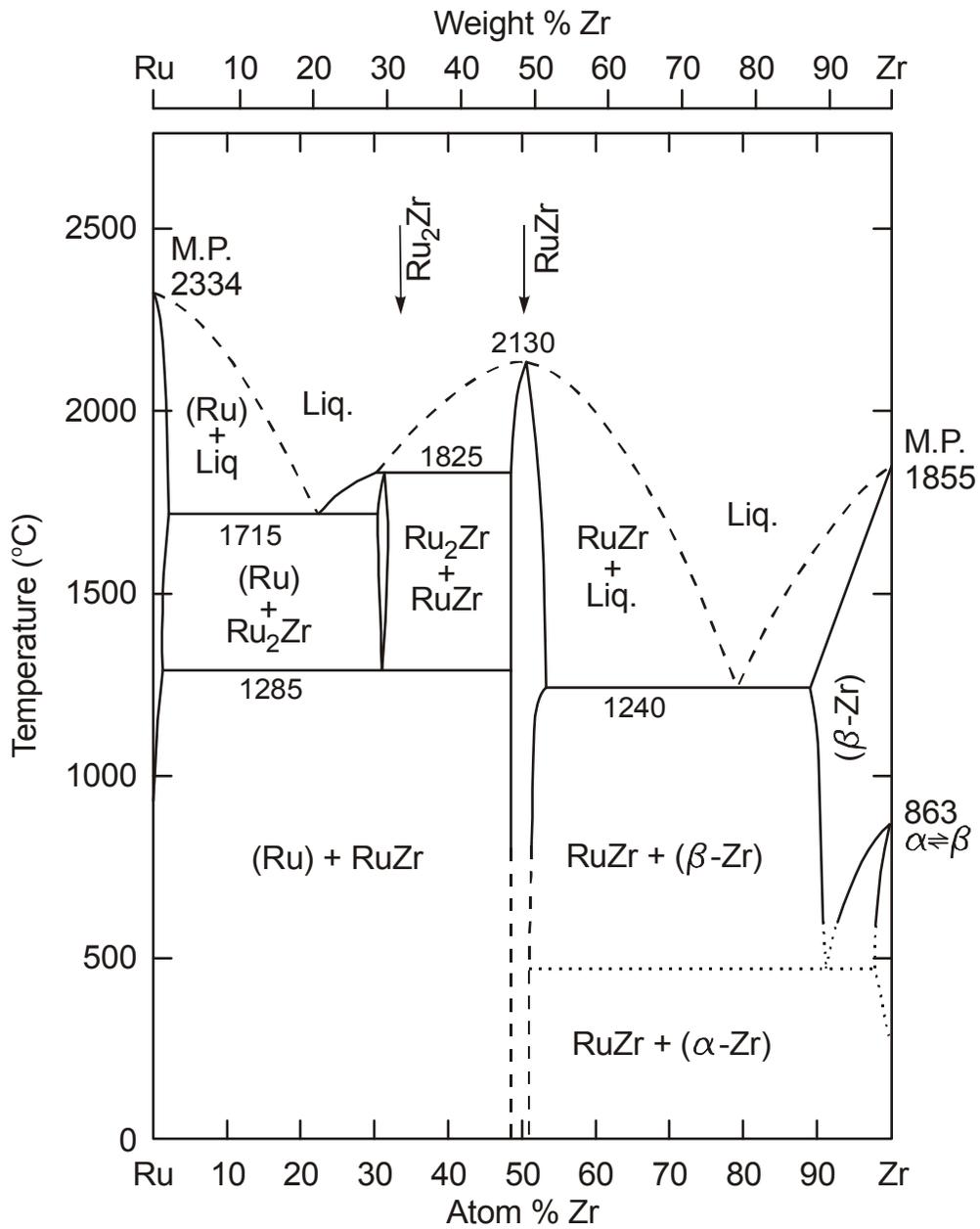
Fig. 10. The Ru-Zr phase diagram.

11. CONCLUSIONS

It appears that observations of Am vaporization from metallic, oxide, and nitride systems are explainable as a result of the thermodynamic analysis developed here and by others. This analysis also indicates that gas-cooled reactor oxide fuels containing americium sesquioxide as a component can probably be manufactured. The key is prevention of americium loss via the gas phase. Figure 1 provides estimates of the maximum temperature and atmosphere at which the gas phase contains $<10^{-8}$ atm of americium species. Processing in a relatively closed system, such as sintering in a crucible having a lid, can also limit volatility losses.

Both plutonium and plutonium-americium oxide fuels will apparently develop in-particle CO pressures of hundreds of atmospheres during burnup to 75% FIMA regardless of the initial O/(Pu+Am) value. An equivalent pressure would be developed by Kr + Xe, and the cesium pressure may reach 78 atm at 1600°C. Failure of the inner pyrocarbon layer would expose SiC to reaction with the high CO pressures and transport silicon away readily as SiO gas.

A plutonium oxycarbide fuel with approximately the same carbide content as the uranium oxycarbide of previous experience will control the CO pressure at negligible levels. However, it appears that an americium-containing oxycarbide fuel cannot be manufactured because of unacceptable americium losses during kernel synthesis.

The rate of corrosion of SiC and ZrC by Pd, Ru, and Rh should be investigated under conditions typical of the driver and transmutation fuels to establish whether previous data applies to these fuels.

The O/f data for coated particles containing actinide oxides has been reviewed and compared with O/f values calculated from the thermodynamics of the fuel oxides, ceria, and urania-gadolinia, with Gd being used as a surrogate for all the Y and lanthanide fission products.

REFERENCES

Ac74 R. J. Ackermann and M. S. Chandrasekharaiah, Proc. Symp. Thermodynamics of Nuclear Materials, 1974, Vienna (1974) 3

Be77 T. M. Besmann and T. B. Lindemer, "Thermodynamic Assessment of the Conversion of Plutonium Dioxide to Plutonium Monocarbide," *J. Nucl. Mater*. **67** (1977) 77-87

Be83 T. M. Besmann and T. B. Lindemer, "Assessment of the Thermodynamic Values for <PuO$_{1.5}$> and High-Temperature Determination of the Values for <PuC$_{1.5}$>," *J. Am. Ceram. Soc.* **66** (11) (1983) 782-785.

Be85 T. M. Besmann and T. B. Lindemer, "Chemical Thermodynamic Representations of <PuO$_{2-x}$> and <U$_{1-z}$Pu$_z$O$_w$>," *J. Nucl. Mater.* **130** (1985) 489-504

Be86 T. M. Besmann and T. B. Lindemer, "Improvement in the Chemical Thermodynamic Representation of <PuO$_{2-x}$> and <U$_{1-z}$Pu$_z$O$_w$>," *J. Nucl. Mater.* **137** (198) 292-293

Be87 T. M. Besmann, "Phase Equilibria and Thermodynamics of the Pu-O system: 1400 K to 1610 K," *J. Nucl. Mater*. **144** (1987) 141-150

Bh96 K. Bhanumurthy and R. Schmid-Fetzer, "Experimental Study of Ternary Pd-Si-C Phase Equilibria and Pd/SiC Interface Interactions," *Z. Metallkd*. **87** (4) (1996) 244-253

Br61 L. Brewer and G. M. Rosenblatt, "Dissociation Energies of Gaseous Metal Dioxides," *Chemical Reviews*, **61** (1) (1961) 257-263

Bu83 R. E. Bullock and J. L. Kaae, "Performance of Coated UO$_2$ Particles Gettered with ZrC," *J. Nucl. Mater*. **115** (1983) 69-83

Bu84 R. E. Bullock, "Fission-Product Release During Postirradiation Annealing of Several Types of Coated Fuel Particles," *J. Nucl. Mater*. **125** (1984) 304-319

Co90 E. H. P. Cordfunke, R. J. M. Konings, G. Prins, P. E. Potter and M. H. Rand, *Thermochemical Data for Reactor Materials and Fission Products*, Elsevier Science Publishing Co., Inc., New York, ISBN
0-444-88485-8, 1990 (Note that the values for ΔG^o_f (Cs$_2$O,s) are incorrect; ΔS^o_f was calculated from S (Cs$_2$O) - 0.5 S (O$_2$) - S (Cs). These values can be corrected by subtracting an additional S (Cs) to give a resulting ΔS^o_f = - 30.09 cal/mol/K or - 125.9 J/mol/K).

Da53 L. S. Darken and R. W Gurry, *Physical Chemistry of Metals*, Figure 14-4, McGraw-Hill Book Co., Inc., New York 1953

En93 T. R. England and B. F. Rider, "Evaluation and Compilation of Fission Product Yields 1993," Los Alamos National Laboratory Report LA-UR-94-3106/ENDF-349 October 1994

Er88 V. N. Eremenko, V. G. Khoruzhaya and T. D. Shtepa, "Temperature of Nonvariant Equilibria in the Systems Zr-Ru and Ru-Ir," *Russian Metallurgy (Metally)* 1988 (1) 194-198. From W. G. Moffatt, *The Handbook of Binary Phase Diagrams*, Genium Publishing Corp., Schenectady, New York 1984

Gr77 H. Grubmeier, A. Naoumidis and B. A. Thiele, "Silicon Carbide Corrosion in High-Temperature Gas-Cooled Reactor Fuel Particles," *Nucl. Technol.* **35** (2) (1977) 413-427

Gr80a D. W. Green, "Relationship Between Spectroscopic Data and Thermodynamic Functions: Application to Uranium, Plutonium, and Thorium Oxide Vapor Species," *J. Nucl. Mater.* **88** (1980) 51-63

Gr80b D. W. Green, "Standard Enthallpies of Formation of Gaseous Thorium, Uranium, and Plutonium Oxides," *Int'l. J. Thermophysics*, **1** (1980) 61-71

Gr82 D. W. Green and L. Leibowitz, "Vapor Pressures and Vapor Compositions in Equilibrium with Hypostoichiometric Uranium Dioxide at High Temperatures," *J. Nucl. Mater.* **105** (1982) 184-195

Gr83 D. W. Green, J. K. Fink and L. Leibowitz, "Vapor Pressures and Vapor Compositions in Equilibrium with Hypostoiciometric Plutonium Dioxide at High Temperatures," pp. 123-143 in Am. Chem. Soc. Symp. Series, No. 216, Plutonium Chemistry (1983)

Ho77 F. J. Homan, T. B. Lindemer, E. L. Long, Jr., T. N. Tiegs and R. L. Beatty, "Stoichiometric Effects on Performance of High-Temperature Gas-Cooled Reactor Fuels from the U-C-O System," *Nucl. Technol.* **35** (2) (1977) 428-441

Hu73 R. Hultgren, P. D. Desai, D. T. Hawkins, M. Gleiser, K. K. Kelley and D. D. Wagman, *Selected Values of the Thermodynamic Properties of the Elements*, American Society for Metals, Metals Park, Ohio 1973

Ka60 S. Katcoff, "Fission-Product Yields from Neutron-Induced Fission," *Nucleonics* **18** (11) (1960) 201-208

Kl85 H. Kleykamp, "The Chemical State of the Fission Products in Oxide Fuels," *J. Nucl. Mater.* **131** (1985) 221-246

Ku79 O. Kubaschewski and C. B. Alcock, *Metallurgical Thermochemistry*, Pergamon Press, Oxford, 1979

La81 H. Langer and E. Wachtel, "Aufbau und Magnetische Eigenschaften von Palladium-Silicium-Legierungen im Konzentrationsintervall 30 bis 100 At.-%Si," *Z. Metallkund.* **72** (1981) 769-775. From W. G. Moffatt, *The Handbook of Binary Phase Diagrams*, Genium Publishing Corp., Schenectady, New York 1984

La84 R. J. Lauf, T. B. Lindemer and R. L. Pearson, "Out-Of-Reactor Studies of Fission Product-Silicon Carbide Interactions in HTGR Fuel Particles," *J. Nucl. Mater.* **120** (1984) 6-30

La87 R. H. Lamoreaux, D. L. Hildenbrand and L. Brewer, "High-Temperature Vaporization Behavior of Oxides II. Oxides of Be, Mg, Ca, Sr, Ba, B, Al, Ga, In, Tl, Si, Ge, Sn, Pb, Zn, Cd, and Hg," *J. Chem. Ref. Data* **16** (3) (1987) 419-443

Li71 T. B. Lindemer and R. A. Bradley, "Kinetic Models for the Synthesis of $(U,Pu)O_{2-y}$ by Hydrogen-Reduction and Carbothermic Techniques," *J. Nucl. Mater.* **41** (1971) 293-302

Li77 T. B. Lindemer, "Measurement and Interpretation of CO and Kr+Xe in Irradiated ThO_2-Containing HTGR Fuel Particles," *J. Am. Ceram. Soc.* **60** (9-10) (1977) 409-416

Li81 T. B. Lindemer, T. M. Besmann and C. E. Johnson, "Thermodynamic Review and Calculations—Alkali-Metal Oxide Systems with Nuclear Fuels, Fission Products, and Structural Materials," *J. Nucl. Mater*. **100** (1-3) (1981) 178-226

Li86a T. B. Lindemer and J. Brynestad, "Review and Chemical Thermodynamic Representation of $U_{1-z}Ce_zO_{2\pm x}$ and $U_{1-z}Ln_zO_{2\pm x}$; Ln = Y, La, Nd, Gd," *J. Am. Ceram. Soc*. **69** (1986) 867-876

Li86b T. B. Lindemer, "Chemical Thermodynamic Representation of Very Nonstoichiometric Phases: $<CeO_{2-x}>$," *CALPHAD* **10** (2) (1986) 129-136

Li86c B. Lindblom and E. Rosen, "Solid State emf Measurements and Phase Studies in the System SrO/Mo/O in the Temperature Range 1200-1600 K," *Acta Chem. Scand* **A40** (1986) 452-458

Li88 T. B. Lindemer, "Study of Nonstoichiometry of $U_{1-z}Gd_zO_{2\pm x}$," *J. Am. Ceram. Soc*. **71** (1988) 553-561

Lo80 R. Lorenzelli and B Touzelin, *J. Nucl. Mater*. **95** (1980) 290-302

Mi90 K. Minato, T. Ogawa, S. Kashimura, K. Fukuda, M. Shimizu, Y. Tayama and I. Takahashi, "Fission Product Palladium-Silicon Carbide Interaction in HTGR Fuel Particles," *J. Nucl. Mater*. **172** (1990) 184-196

Mi91 K. Minato, T. Ogawa, S. Kashimura, K. Fukuda, I. Takahashi, M. Shimizu and Y. Tayama, "Carbon Monoxide-Silicon Carbide Interaction in HTGR Fuel Particles," *J. Mater. Sci*. **26** (1991) 2379-2388

Mi00 K. Minato, T. Ogawa, K. Sawa, A. Ishikawa, T. Tomita, S. Iida and H. Sekino, "Irradiation Experiment on ZrC-Coated Fuel Particles for High-Temperature Gas-Cooled Reactors," *Nucl. Technol*. **130** (2000) 272-281

Og86 T. Ogawa and K. Ikawa, "Reactions of Pd with SiC and ZrC," *High Temp. Sci*. **22** (1986) 179-193

Og95 T. Ogawa, T. Ohmichi, A. Maeda, Y. Arai and Y. Suzuki, "Vaporization Behaviour of (Pu,Am)N," *J. of Alloys and Compounds* **224** (1995) 55-5

Oz73 P. I. Ozhegov, B. F. Myasoedov and E. A. Zakharov, translated from Doklady Akademii Nauk SSSR 212 (5) (1973) 1122-1124

Pa82 L. B. Pankratz, *Thermodynamic Properties of the Elements and Oxides*, U. S. Dept. Interior Bureau of Mines Bull. 672 (U. S. Govt. Printing Office, Washington DC 1982)

Pe79   R. L. Pearson and T. B. Lindemer, "Simulated Fission Product Oxide Behavior in Triso-Coated HTGR Fuel", Oak Ridge National Laboratory Report ORNL/TM-6741 (1979).

Pe80   R. L. Pearson and T. B. Lindemer, "Simulated Fission Product-SiC Interaction in Triso-Coated LEU or MEU HTGR Fuel Particles", Oak Ridge National Laboratory Report ORNL/TM-6741 (1980).

Pe83 J. B. Pedley and E. M. Marshall, "Thermochemical Data for Gaseous Monoxides," *J. Phys. Chem. Ref. Data* **12** (4) (1983) 967-996

Pr82 E. Proksch, A. Strigl and H Nabielek, "Production of Carbon Monoxide During Burn-Up of UO_2 Kerneled HTR Fuel Particles," *J. Nucl. Mater*. **107** (1982) 280-285

Pr85 E. Proksch, A. Strigl and H Nabielek, "Production of Carbon Monoxide During Burn-Up of $(Th,U)O_2$ Kerneled HTR Fuel Particles," *J. Nucl. Mater*. **136** (1985) 129-135

Ri78 K. Richter, "Method for Preparation of Plutonium Carbide," Luxembourg Patent 79,020, June 21, 1978.

Ro95 R. S. Roth, Ed., *Phase Diagrams for Ceramists*, Volume XI, Fig. 9180. (1995) The American Ceramic Society, Westerville, Ohio 43081

Ro02 C. Rodriguez, et al,. "Deep Burn Transmutation of Nuclear Waste", HTR 2002 Proceedings, 1st International Topical Meeting High Temperature Reactor Technology, April 2002, Petten, Netherlands.

Sa68 C. Sari, U. Benedict and H. Blank, Proc. Symp. on the Thermodynamics of Nuclear Materials 1967, Vienna (IAEA, Vienna, 1968) 587-611

Sa71 E. M. Savitskii, V. P. Polyakova, B. P. Krivdin, A. A. Kozlov and E. M. Khorlin, "Phase Diagrams of Platinum and Palladium with Barium, Scandium, and Zirconium," *Diagr. Sost. Met. Sistem*, Nauka, Moscow (1971) 200-203. From W. G. Moffatt, *The Handbook of Binary Phase Diagrams*, Genium Publishing Corp., Schenectady, New York 1984

St71 D. R. Stull and H. Prophet, JANAF Thermochemical Tables, NSRDS-NBS-37, (1971) U. S. Government Printing Office, Washington DC

Tr93 C. L. Trybus, J. E. Sanecki and S. P. Henslee, "Casting of metallic fuel containing minor actinide additions," *J. Nucl. Mater*. **204** (1993) 50-55

Wy81 J. A. Wysocki and P. E. Duwez, "Equilibrium Silicides of Palladium," *Met. Trans. A*, **12A** (1981) 1455-1460. From W. G. Moffatt, *The Handbook of Binary Phase Diagrams*, Genium Publishing Corp., Schenectady, New York 1984

APPENDIX 1. COLLECTED THERMODYNAMIC DATA

APPENDIX 1. COLLECTED THERMODYNAMIC DATA

The following expressions are generally valid over $1000 < T\ (K) < 2000$ except as noted.

ΔG^o_f of the elements in their standard states is zero

ΔG^o_f (Am,g) (cal/mol) = 65,345 - 29.88T, T < 1448 K

ΔG^o_f (Am,g) (cal/mol) = 58,076 - 24.86T, T > 1448 K

ΔG^o_f (AmO,g) (cal/mol) = - 14,000 - 20.26T

ΔG^o_f (AmO$_2$,g) (cal/mol)= - 98,000 - 2.32T

ΔG^o_f (AmO$_2$) (cal/mol) = - 220,030 + 41.41T

ΔG^o_f (Am$_2$O$_3$) (cal/mol) = - 396,618 + 50.93 T

ΔG^o_f (AmC$_{1.5}$) = ΔG^o_f (PuC$_{1.5}$) (cal/mol) = - 21,370 + 2.06T

ΔG^o_f (AmN) (cal/mol) = - 71,140 + 22.0T

ΔG^o_f (CO) (cal/mol) = - 27,095 - 20.764T

ΔG^o_f (H$_2$O) (cal/mol) = - 59,679 + 13.64T

ΔG^o_f (O,g) (cal/mol) = 60,668 - 15.793T

ΔG^o_f (Pu,g) (cal/mol) = 78,110 - 21.23T, T > 913 K

ΔG^o_f (PuO,g) (cal/mol) = - 28,500 - 9.7T

ΔG^o_f (PuO$_2$,g) (cal/mol) = - 112,600 + 6.6T

 (see refs. gr83, gr82, gr80a, and gr80b for new assessments for the previous two values)

ΔG^o_f (PuO$_2$) (cal/mol) = - 250,430 + 44.86T

ΔG^o_f (Pu$_2$O$_3$) (cal/mol) = - 399,600 + 63.8T

ΔG^o_f (PuC$_{1.5}$) (cal/mol) = - 21,370 + 2.06T

ΔG^o_f (SiO$_2$) (cal/mol) = - 215,430 + 40.90T (for cristobalite)

ΔG^o_f (SiO,g) (cal/mol) = - 25,298 - 19.184T

ΔG^o_f (SiC) (cal/mol) = - 17,029 + 1.84T

ΔG^o_f (SrO) (cal/mol) = - 142,436 + 24.813T

ΔG^o_f (Sr$_2$MoO$_4$) (cal/mol) = - 443,032 + 86.726T

ΔG^o_f (SrMoO$_4$) (cal/mol) = - 363,750 + 77.93T, 1000-1600 K

ΔG^o_f (Sr$_2$MoO$_4$) (cal/mol) = - 293,671 + 59.51T, 1000-1600 K

INTERNAL DISTRIBUTION

1. C. A. Baldwin	12. J. B. Knauer
2. S. J. Ball	13. R. A. Lowden
3. G. L. Bell	14. G. E. Michaels
4. T. M. Besmann	15. F. L. Montgomery
5. E. E. Bloom	16. R. N. Morris
6. E. D. Collins	17. K. R. Thoms
7. B. S. Cowell	18–22. D. F. Williams
8. G. D. Del Cul	23. Central Research Library
9. L. K. Felker	24. ORNL Laboratory Records – RC
10. R. G. Haire	25. ORNL Lab Records - OSTI
11. D. J. Hill	

EXTERNAL DISTRIBUTION

26. M. D. Allendorf, Sandia National Laboratories, Mail Stop 9052, Livermore, CA 94551-0969
27. W. B. Boore, Westinghouse Savannah River Company, P.O. Box 616, Bldg. 703-45A, Rm. 250, Aiken, SC 29802
28. D. Bowers, Argonne National Laboratory – East, 9700 S. Cass Avenue, Argonne, IL 60439
29. J. C. Bresee, U.S. Department of Energy – NE-30, Office of Advanced Accelerator Applications, FORS, 1000 Independence Ave. SW, Washington, DC 20585
30. K.Chidester, Los Alamos National Laboratory, H816, P.O. Box 1663, Los Alamos, NM 87545
31. D. C. Crawford, Argonne National Laboratory – West, P.O. Box 2528, Idaho Falls, ID 83403
32. Y. Degaltsev, Russian Research Center, Kurchatov Institute (RRC-KI), Kurchatov Square – 1, 123182, Moscow, Russian Federation (degal@adis.vver.kiae.ru)
33. P. J. Finck, Argonne National Laboratory – East, 9700 S. Cass Avenue, Bldg. TD360, Rm. L120A, Argonne, IL 60439
34. F. J. Goldner, U.S. Department of Energy – NE-30, Office of Advanced Accelerator Applications, FORS, 1000 Independence Ave SW, Washington, DC 20585
35. I. Golubev, A.A. Bochvar All-Russia Research Institute of Inorganic Materials (VNIINM), Rogov str.5, Moscow 123060, Box 369, Russian Federation (golubev@bochvar.ru)
36. D. Hanson, General Atomics, P.O. Box 85608, 3550 General Atomics Court, San Diego, CA 92121-1194
37. M. Harbach, Harbach Engineering and Solutions, Inc., 8807 Fox Hollow Court, Dayton OH 45458
38. S. Hayes, Argonne National Laboratory – West, P.O. Box 2528, Idaho Falls, ID 83403
39. J. Herczeg, U.S. Department of Energy – NE-20, Office of Technology and International Cooperation, FORS, 1000 Independence Ave SW, Washington, DC 20585
40. F. J. Homan, 7501 Wickam Rd., Knoxville, TN 37931
41. I. Kadermetov, A.A. Bochvar All-Russia Research Institute of Inorganic Materials (VNIINM), Rogov str.5, Moscow 123060, Box 369, Russian Federation (kadar@bochvar.ru)
42. M. Kania, Knolls Atomic Power Laboratory, P.O. Box 1072, Bin 154, Schenectady, NY 12301-4422
43. P. Karcz, U. S. Department of Energy, NNSA/NA-263, Office of International Technology, FORS, 1000 Independence Ave. SW, Washington, DC 20585

44. J. J. Laidler, Argonne National Laboratory – East, 9700 S. Cass Avenue, Bldg. 205/CMT, Argonne, IL 60439
45. J. Lambert, Argonne National Laboratory – East, 9700 S. Cass Avenue, Argonne, IL 60439
46. L. Lebowitz, Argonne National Laboratory – East, 9700 S. Cass Avenue, Argonne, IL 60439
47. T. B. Lindemer, 10931 Sallings Rd., Knoxville, TN 37922
48. A. L. Lotts, 11125 Hatteras Dr., Knoxville, TN 37922
49. V. M. Makarov, A.A. Bochvar All-Russia Research Institute of Inorganic Materials (VNIINM), Rogov str.5, Moscow 123060, Box 369, Russian Federation (makarov@bochvar.ru)
50. R. Margevicius, Los Alamos National Laboratory, P.O. Box 1663, Los Alamos, NM 87545
51. S. McDeavitt, Argonne National Laboratory – East, 9700 S. Cass Avenue, Argonne, IL 60439
52. D. McEachern, General Atomics, P.O. Box 85608, 3550 General Atomics Court, San Diego, CA 92121-1194
53. M. Meyer, Argonne National Laboratory – West, P.O. Box 2528, Idaho Falls, ID 83403
54. K. Minato, Research Group for Actinides Science, Department of Materials Science, Japan Atomic Energy Research Institute, Tokai-mura, Ibaraki-ken 319-1195, Japan (minato@popsvr.tokai.jaeri.go.jp)
55. H. Nabielik –KFA Juelich (h.nabielik@fz-juelich.de)
56. M. Richards, General Atomics, P.O. Box 85608, 3550 General Atomics Court, San Diego, CA 92121-1194
57. P. Rittenhouse, 346 Myers Rd., Kingston, TN 37763
58. C. Rodriguez , General Atomics, P.O. Box 85608, 3550 General Atomics Court, San Diego, CA 92121-1194
59. J. Runge, Argonne National Laboratory – East, 9700 S. Cass Avenue, Argonne, IL 60439
60. J. Saurwein, General Atomics, P.O. Box 85608, 3550 General Atomics Court, San Diego, CA 92121-1194
61. B. Scheffel, General Atomics, P.O. Box 85608, 3550 General Atomics Court, San Diego, CA 92121-1194
62. S. Shiozawa, Japan Atomic Energy Research Institute, Oarai Research Establishment, 3607 Niibori, Narita-cho, Oarai-machi, Higashi-Ibaraki-gun, Ibaraki-ken 311-1394, Japan (shsh@spa.oarai.jaeri.go.jp)
63. O. Stansfield, 42 Rivers Run Way, Oak Ridge, TN 37830
64. I. Suslov, OKBM – Burnakovsky proead, 15, Nizhny Novogrod-74, Russia 603603 (suslov@okbm.nnov.ru)
65. R. P. Wichner, 104 Burgess Ln., Oak Ridge, TN 37830-7833
66. M. A. Williamson, Argonne National Laboratory – East, 9700 S. Cass Avenue, Argonne, IL 60439